American Society of Hematology
2021 L Street NW, Suite 900,
Washington, DC 20036
Phone: 202-776-0544 | Fax 202-776-0545
editorial@hematology.org

DHODH as a Targetable Metabolic Achilles' Heel for chemo-resistant B-ALL

Tracking no: BLD-2025-029264R2

Yuxuan Liu (Stanford University, United States) Haowen Jiang (Stanford University, United States) Jingjing Liu (St. Jude Children's Research Hospital, United States) Lucille Stuani (INSERM, France) Milton Merchant (Stanford University, United States) Astraea Jager (Stanford University, United States) Abhishek Koladiya (Stanford University, United States) Ti-Cheng Chang (St. Jude Children's Research Hospital, United States) Pablo Domizi (Stanford University, United States) Jolanda Sarno (University of Milan-Bicocca, Italy) Ao Wang (Stanford University, United States) Timothy Keyes (Stanford Health Care, United States) Dorra Jedoui (Stanford University, United States) Jodie Meng (Stanford University, United States) Felix Hartmann (German Cancer Research Center (DKFZ), Germany) Ruida Hou (St. Jude Children's Research Hospital, United States) Carol Fries (University of Rochester, United States) Chiara Pirillo (Stanford University, United States) Qingsong Gao (St. Jude Children's Research Hospital, United States) Ilaria Iacobucci (St. Jude Children's Research Hospital, United States) Sean Bendall (Stanford University, United States) Min Huang (Stanford University, United States) Norman Lacayo (Stanford University School of Medicine, United States) Kathleen Sakamoto (Stanford University School of Medicine, United States) Charles Mullighan (St Jude Children's Research Hospital, United States) Mignon Loh (Seattle Children's Hospital, the Ben Town Center for Childhood Cancer Research, University of Washington, Seattle, WA., United States) Jiyang Yu (St. Jude Children's Research Hospital, United States) Jun Yang (St. Jude Children's Research Hospital, United States) Jiangbin Ye (Department of Radiation Oncology, Stanford University School of Medicine. Stanford, CA, United States) Kara Davis (Stanford University, United States)

Abstract:
Relapse remains a major barrier to survival in B-cell acute lymphoblastic leukemia (B-ALL). Both activation of B-cell signaling pathways and increased glucose consumption have been linked to chemo-resistance and relapse risk. Here, we connect these observations, showing that B-ALL cells with active signaling, marked by high phosphorylated ribosomal protein S6 (pS6+), are glucose dependent. Isotope tracing confirms that pS6+ cells are highly glycolytic and rely on glucose for de novo nucleotide synthesis. Uridine, but not other purines or pyrimidines, rescues pS6+ cells from glucose deprivation, highlighting uridine as essential for survival. Active mTOR signaling in pS6+ cells drives de novo pyrimidine synthesis by activating CAD (Carbamoyl phosphate synthetase 2, Aspartate transcarbamylase, and Dihydroorotase), which catalyzes the first steps of de novo pyrimidine synthesis. Inhibiting signaling abolishes glucose dependency and CAD phosphorylation. Primary pS6+ cells express high levels of pyrimidine synthesis proteins, including dihydroorotate dehydrogenase (DHODH), the rate-limiting enzyme in pyrimidine synthesis. Increased DHODH expression correlates with relapse and poor event-free survival. Most B-ALL molecular subtypes exhibit DHODH activity. BAY-2402234, a DHODH inhibitor, effectively kills pS6+ cells in vitro, with IC50 values correlating with pS6 signaling strength across 14 B-ALL patient-derived xenografts (PDX). In vivo, DHODH inhibition prolongs survival and reduces leukemia burden in pS6+ B-ALL models. These findings link active signaling to pyrimidine dependency and relapse risk, highlighting DHODH inhibition as a promising therapeutic strategy for chemo-resistant B-ALL.

Conflict of interest: No COI declared

COI notes:

Preprint server: Yes; biorxiv https://doi.org/10.1101/2025.01.27.635108

Author contributions and disclosures: Y.L. conceived of, designed, and led this study, designed and performed experiments, analyzed and interpreted data, generated the figures, and wrote the manuscript. H.J. conducted experiments and analyzed stable isotope metabolomics data. J.L. performed data analysis for the TARGET and MP2PRT datasets. L.S., A.J., and D.J. contributed to CyTOF experiments and validated the antibody panel used in these experiments. M.M. and C.P. assisted with in vivo mouse studies, cell culture work, retrovirus generation and transduction. A.K. performed the CyTOF data analysis using XGboost. T.C. provided guidance for MP2PRT dataset analysis. P.D. and J.S. performed cell sorting, RNA extraction and performed RNA-seq data analysis. J.M., I.I., Q.G. assisted in genomic analyses. T.K. contributed to developmental classification data analysis using tidytof. A.W. contributed to western blot analysis. F.H. and S.B. provided guidance on CyTOF experiments. M.H., N.J.L, K.M.S., C.G.M., M.L., R.H, C.F., J.Yu. and J.Yang. contributed patient or PDX samples and provided clinical data. H.J., J.L., L.S., P.D., J.Yu., J.Yang. and J.Ye. provided guidance and scientific input. K.L.D. conceived of and designed this study, provided guidance and scientific input, interpreted data, and wrote the manuscript. All authors discussed the results and prepared the manuscript.

Non-author contributions and disclosures: No;

Agreement to Share Publication-Related Data and Data Sharing Statement: CYTOF data from clinically annotated patient samples, cell lines, and PDX samples are available in Community Cytobank (https://community.cytobank.org) under accession numbers 119315 (patients), 119316 (cell lines), 119640, and 119641 (PDX samples) respectively. Bulk RNA-seq data from primary samples in our previously published patient cohort (n=6) have been deposited in NCBI Gene Expression Omnibus (GEO) and are accessible through GEO accession number GSE286115. The TARGET dataset used for this study is accessible through the TARGET website at https://ocg.cancer.gov/programs/target/data-matrix. TARGET BAM and FASTQ sequence files are accessible through the database of genotypes and phenotypes (dbGaP; https://www.ncbi.nlm.nih.gov/projects/gap/cgi-bin/study.cgi?study_id=phs000218.v24.p8) under accession no. phs000218 (TARGET) and at NCI's Genomic Data Commons (http://gdc.cancer.gov) under project TARGET. Transcriptomic data in MP2PRT dataset are accessible in dbGaP: Project ID: MP2PRT-ALL; accession number: phs002005.v1.p1 (https://www.ncbi.nlm.nih.gov/projects/gap/cgi-bin/dataset.cgi?study_id=phs002005.v1.p1).

Clinical trial registration information (if any):

DHODH as a Targetable Metabolic Achilles' Heel for chemo-resistant B-ALL

Yuxuan Liu*[1], Haowen Jiang[2], Jingjing Liu[3], Lucille Stuani[4], Milton Merchant[1], Astraea Jager[1], Abhishek Koladiya[1], Ti-Cheng Chang[5], Pablo Domizi[1], Jolanda Sarno[1,6], Ao Wang[1], Timothy Keyes[1], Dorra Jedoui[1], Jodie Meng[1], Felix Hartmann[7], Ruida Hou[8], Carol Fries[9], Chiara Pirillo[1], Qingsong Gao[10], Ilaria Iacobucci[10], Sean C. Bendall[11], Min Huang[1], Norman J. Lacayo[1], Kathleen M. Sakamoto[1], Charles G. Mullighan[10], Mignon Loh[12], Jiyang Yu[3], Jun J. Yang[8], Jiangbin Ye[2], Kara L. Davis*[1,13]

[1] Division of Hematology, Oncology, and Stem Cell Transplant and Regenerative Medicine, Department of Pediatrics, Stanford University, CA
[2] Department of Radiation Oncology, Stanford University School of Medicine. Stanford, CA
[3] Department of Computational Biology, St. Jude Children's Research Hospital, Memphis, TN
[4] Institut de Recherche en Cancérologie de Montpellier (IRCM), INSERM; Univ. Montpellier, Institut régional du Cancer de Montpellier (ICM), Montpellier, France
[5] Center for Applied Bioinformatics, St Jude Children's Research Hospital, Memphis, TN
[6] School of Medicine and Surgery, University of Milan-Bicocca, Milan, Italy
[7] Systems Immunology and Single-Cell Biology, German Cancer Research Center (DKFZ), Heidelberg, Germany
[8] Division of Pharmaceutical Sciences, Department of Pharmacy and Pharmaceutical Sciences, St. Jude Children's Research Hospital, Memphis, TN
[9] Department of Pediatrics, Pediatric Hematology/Oncology, University of Rochester, Rochester, NY, USA
[10] Department of Pathology, St. Jude Children's Research Hospital, Memphis, TN
[11] Department of Pathology, Stanford University, Stanford, CA
[12] Department of Pediatrics and Ben Towne Center for Childhood Cancer Research, Seattle Children's Hospital, University of Washington, Seattle, WA
[13] Center for Cancer Cell Therapy, Stanford Cancer Institute, Stanford University School of Medicine, Stanford, CA

*Correspondence: yuxuan31@stanford.edu; kardavis@stanford.edu

Short title: DHODH in B-ALL

Text word count: 3,953

Abstract word count: 228

Number of Figures: 6

Number of references: 64

Key points

1. Relapse-associated B-ALL cells with active mTOR signaling rely on glucose for pyrimidine synthesis, with DHODH expression linked to poor outcomes.

2. DHODH inhibition kills B-ALL cells with active mTOR signaling, reduces leukemia burden and offers a therapeutic strategy in B-ALL.

Abstract

Relapse remains a major barrier to survival in B-cell acute lymphoblastic leukemia (B-ALL). Both activation of B-cell signaling pathways and increased glucose consumption have been linked to chemo-resistance and relapse risk. Here, we connect these observations, showing that B-ALL cells with active signaling, marked by high phosphorylated ribosomal protein S6 (pS6+), are glucose dependent. Isotope tracing confirms that pS6+ cells are highly glycolytic and rely on glucose for *de novo* nucleotide synthesis. Uridine, but not other purines or pyrimidines, rescues pS6+ cells from glucose deprivation, highlighting uridine as essential for survival. Active mTOR signaling in pS6+ cells drives *de novo* pyrimidine synthesis by activating CAD (Carbamoyl phosphate synthetase 2, Aspartate transcarbamylase, and Dihydroorotase), which catalyzes the first steps of *de novo* pyrimidine synthesis. Inhibiting signaling abolishes glucose dependency and CAD phosphorylation. Primary pS6+ cells express high levels of pyrimidine synthesis proteins, including dihydroorotate dehydrogenase (DHODH), the rate-limiting enzyme in pyrimidine synthesis. Increased DHODH expression correlates with relapse and poor event-free survival. Most B-ALL molecular subtypes exhibit DHODH activity. BAY-2402234, a DHODH inhibitor, effectively kills pS6+ cells in vitro, with IC50 values correlating with pS6 signaling strength across 14 B-ALL patient-derived xenografts (PDX). In vivo, DHODH inhibition prolongs survival and reduces leukemia burden in pS6+ B-ALL models. These findings link active signaling to pyrimidine dependency and relapse risk, highlighting DHODH inhibition as a promising therapeutic strategy for chemo-resistant B-ALL.

Introduction

Metabolic dysregulation is a hallmark of cancer with roles in tumor initiation, progression, and chemotherapy resistance[1-3]. Warburg first described cancer cells favoring glycolysis to produce lactate over oxidative phosphorylation even with sufficient oxygen[4]. The understanding of cancer-specific metabolic adaptations has led to new insights into cancer biology and therapies, such as targeting isocitrate dehydrogenase (IDH) mutations in leukemia and gliomas[5-9]. However, the role of dysregulated metabolism in acute lymphoblastic leukemia (ALL) remains incompletely understood.

ALL is a cancer composed of immature lymphocytes, most commonly of the B lineage. ALL primarily affects children but has a worse prognosis in adolescents and adults due to high-risk genomic features and relapse susceptibility.[10-12] To better understand ALL cells capable of mediating relapse, we identified a subset of pre-B-like ALL cells characterized by phosphorylation of several proteins in PI3K/mTOR signaling pathway: ribosomal protein S6 (pS6), 4EBP1, CREB, SYK, collectively termed "pS6+ cells," whose presence at diagnosis strongly predict relapse[13]. While active IL-7 receptor (IL-7R) and pre-B cell receptor (pre-BCR) signaling in B-cell developmental pathways contribute to the pathogenesis and prognosis of ALL,[14-17] targeting these pathways has not been a successful therapeutic strategy.

Here, we demonstrate that pS6+ cells possess a unique metabolic dependency using glucose for pentose phosphate pathway (PPP) and *de novo* pyrimidine synthesis to produce uridine, driven by mTOR-mediated CAD phosphorylation. This dependency correlates with pS6 signaling strength and is reversed by mTOR inhibition. Gene expression analyses link high expression of pyrimidine synthesis genes to relapse and poor survival in B-ALL. Targeting dihydroorotate dehydrogenase (DHODH), the rate-limiting enzyme in this pathway, demonstrates remarkable efficacy in pS6+ B-ALL models across genetic backgrounds, including those at high relapse risk. Together, these data provide compelling evidence for a novel metabolic intervention relevant to patients at high risk of relapse with B-ALL.

Methods

Information of cell lines, PDX and patient samples are detailed in Supplemental Methods.

Definition of pS6+ and pS6- cell lines and PDXs

The pS6 signaling strength was defined as the arcsinh-transformed median expression value of pS6 profiled by CyTOF. As a cutoff, we defined cell lines and PDXs with pS6 median values greater than 3 as pS6+ and the ones no greater than 3 as pS6-.

NetBID2 analysis to query DHODH activity in patients with B-ALL

We applied NetBID2 algorithm[18,19] to infer DHODH gene activities using bulk RNA-seq data comprising 1,985 B-ALL patients[20]. Using SJARACNe we built a B-ALL interactome (BALLi) with 10,843 hub including 1,937 transcription factors and 8,906 signaling proteins[20]. To ensure robust network quality, we excluded subtypes with fewer than 15 samples. The

parameters for SJARACNe were configured as follows: 1) Bootstrap $p = 1 \times 10^{-7}$; 2) Consensus $p = 1 \times 10^{-5}$; 3) Data Processing Inequality (DPI) tolerance = 0; 4) 100 bootstraps. The resulting data-driven BALLi consisted of 33,237 nodes and 314,914 edges. Gene activity was inferred using cal.Activity function (es.method = "weightedmean" and std = TRUE). The NetBID2 package is available at GitHub.

In vivo DHODHi treatment in cell line and PDX models

NOD/SCID/IL2R$\gamma^{-/-}$ (NSG) female mice (6 to 8-week old) were purchased from The Jackson Laboratory and maintained under the Stanford University Committee on Animal Welfare–approved protocol. Mice were engrafted via IV injection with 5.0×10^5 cells (Nalm6-Luc$^+$, Nalm16-Luc$^+$, SJ18305-Luc$^+$ or SJ45503-Luc$^+$). Upon detectable engraftment (bioluminescence $> 1 \times 10^6$), mice were randomized to vehicle or BAY-2402234 (5mg/kg, 5 days/week, oral gavage). For PDX model, n = 5 (vehicle) and n = 10 (BAY-2402234) with 5 sacrificed at the midpoint (parallel to vehicle leukemia onset) and 5 at the endpoint upon leukemia symptoms. For cell line model, n = 5 per group were monitored for engraftment and survival. Engraftment was assessed via BLI and the frequency of hCD19/hCD45+/mCD45.1- cells in peripheral blood. Mice were sacrificed upon leukemia symptoms. In the survival analysis, one accidental death and one non-engrafted mouse were censored. Nalm16-derived xenograft BM samples (BAY-2402234 n = 4; vehicle n = 5) were profiled by CyTOF.

Statistical analysis

Data were analyzed and visualized using R statistical software (http://www.r-project.org) or GraphPad Prism 10 software. P values were calculated using the statistical test described in the relevant figure legend. $P < 0.05$ was considered statistically significant, and P values are denoted with asterisks as follows ($P > 0.05$, not significant, n.s.; *, $P < 0.05$; **, $P < 0.01$; ***, $P < 0.001$; and ****, $P < 0.0001$).

Please find more detailed methods in the Supplemental Methods.

Results

pS6+ cells have distinct metabolic gene signatures and energetics

Previously, we identified pS6+ cells in B-ALL patients at the time of diagnosis and found them to be associated with future relapse after standard chemotherapy[13]. To identify features distinguishing relapse-associated pS6+ cells from pS6- cells in continuous remission, we sorted pre-B cells from six diagnostic bone marrow (BM) samples with known pS6 status from our previously published B-ALL cohort (n = 3 pS6+; n = 3 pS6-; Supplemental Table 1-2) for whole transcriptomic sequencing (Figure 1A, Supplemental Figure 1A-B). Pathway analysis demonstrated enrichment in mTORC1 and PI3K/Akt/mTOR signaling pathways in pS6+ cells, consistent with our published proteomic signature[13], along with higher expression of MYC gene targets and metabolic gene pathways, e.g. oxidative phosphorylation (OXPHOS), glycolysis, and fatty acid metabolism (Figure 1B, Supplemental Table 3). These data confirmed the activation of PI3K/mTOR signaling we previously observed by proteomic analysis and suggested this signaling is associated with a unique metabolic state.

Using mass cytometry (CyTOF), we profiled nine B-ALL cell lines and categorized them as pS6+ or pS6- cells based on pS6 signaling strength (Figure 1C). pS6+ cells exhibited higher expression of pERK ($p = 0.004$), pAKT, p4EBP1, and pCREB (all $p = 0.095$, ns), as shown in Figure 1D. Metabolic flux confirmed $pS6^+$ cells exhibit greater glycolysis and OXPHOS activity than $pS6^-$ cells, reflected in extracellular acidification rate (ECAR, $p = 0.0039$) and oxygen consumption rate (OCR, $p = 0.0191$; Figure 1E, Supplemental Figure 2A), both correlating with $pS6^+$ cell frequency (ECAR $p = 0.021$; OCR $p = 0.0068$; Figure 1F, Supplemental Figure 2B). Thus, as suggested by the transcriptomic analysis of primary cells, pS6+ cells have higher metabolic activity than pS6- cells, which is directly correlated to their frequency.

pS6+ cells utilize glucose to fuel *de novo* pyrimidine synthesis

Glucose and glutamine are primary carbon sources for glycolysis and OXPHOS in cancer[21]. Under glucose deprivation, pS6+ cells showed significant cell death after 48 hours (Nalm6 $p = 0.00098$; 697 $p = 0.0064$; Kasumi2 $p = 0.0022$; Nalm16 $p = 0.026$; REH $p = 0.018$; Figure 1G), whereas pS6- cells were largely unaffected (RS4;11 $p = 0.61$; MHH-CALL-4 $p = 0.52$; Nalm20 $p = 0.08$; Figure 1G). Glutamine deprivation had no impact except in Nalm6 cells (Supplemental Figure 2C).

To understand how pS6+ cells utilize glucose, we performed isotype tracing[22] with U-^{13}C-glucose in the absence of glutamine in pS6+ and pS6- cells. pS6+ cells distinctly

incorporated ^{13}C-glucose into metabolites in the glycolysis, PPP and the TCA cycle as illustrated schematically in Figure 2A. We did not observe significant differences in fractional ^{13}C labeling of intermediates in glycolysis and TCA cycle between pS6+ and pS6- cells (Supplemental Figure 3-4). Yet, pS6+ cells had significantly higher fractional ^{13}C labeling in m+5 UDP ($p = 0.0233$), UTP ($p = 0.002$), and ATP ($p = 0.0342$) compared to pS6- cells (Figure 2B), suggesting pS6+ cells are using glucose for PPP and nucleotide production. Moreover, rescue experiments demonstrated uridine, as the first pyrimidine nucleoside product, most effectively rescued pS6+ cells from glucose deprivation (Nalm6 and 697, $p < 0.0001$; Nalm16, $p = 0.0002$; REH, $p = 0.0485$, Figure 2C) while, as expected, there was no impact in pS6- cells. Pyruvate provided partial rescue against cell death in two cell lines (697, $p = 0.0007$; Nalm16, $p = 0.016$), indicating it can support glycolysis and TCA cycle flux as a key metabolite but is not sufficient for complete metabolic compensation. Other metabolites, including aspartate, pyrimidine, and purine failed to rescue cells from death, highlighting glucose-dependent pyrimidine synthesis as a critical vulnerability in pS6+ B-ALL cells.

PI3K/mTOR pathway activation drives pyrimidine synthesis

S6 kinase (S6K1) is a tyrosine kinase situated downstream of the PI3K/mTOR pathway that phosphorylates ribosomal protein S6, thus making pS6 a proxy for PI3K/mTOR pathway activity (Supplemental Figure 5A). S6 kinase also phosphorylates and activates CAD[23,24]. CAD catalyzes the initial steps in *de novo* pyrimidine synthesis to produce UMP and uridine (Figure 2D). We found higher phosphorylated CAD (pCAD) in pS6+ cells compared to pS6- cells (Figure 2D). To study if the PI3K/mTOR pathway drives *de novo* pyrimidine synthesis through pCAD, we tested tyrosine kinase inhibitors (TKIs) targeting kinases in the PI3K/mTOR pathway (S6 kinase, PI3K, mTOR, SYK). We confirmed inhibition of downstream signaling nodes using CyTOF (Supplemental Figure 5B). We found that pCAD is inhibited after treatment with TKIs targeting several levels of the PI3K/mTOR network in pS6+ cell lines and PDXs (Figure 2E, Supplemental Figure 5C). To understand how kinase inhibition influences glucose utilization and dependency, we evaluated glycolytic activity and glucose sensitivity after TKI treatment *in vitro*. SYK inhibition, one of the upstream proteins in the signaling pathway, significantly decreased ECAR in pS6+ cells, but not in pS6- cells (Supplemental Figure 5D-E). SYK, mTOR, or PI3K inhibition alleviated the glucose dependency in pS6+ cells (Supplemental Figure 5F). These

findings indicate that the active PI3K/mTOR signaling that characterizes pS6+ cells governs glucose dependency driving *de novo* pyrimidine synthesis through regulation of pCAD.

Given mTOR is a known upstream regulator of pS6 signaling and *de novo* pyrimidine synthesis[23,24], we investigated its role in the context of B-ALL. Pretreatment with an mTOR inhibitor (rapamycin), but not S6K1 inhibitor (PF-4708671), abrogated the sensitivity to DHODH inhibition (DHODHi) (Supplemental Fig. 6A) demonstrating that mTOR, rather than S6K1, is the critical driver of pyrimidine dependency. To further confirm the role of S6K1 and pS6 in pyrimidine synthesis, we generated pS6-inactive *RPS6KB1* (S6K1) CRISPR knockout cells in Nalm6, 697 and REH. S6K1 KO cells exhibited reduced pCAD and pS6 compared to wildtype cells (Supplemental Figure 6B). Next, we evaluated their response to inhibition of DHODH, the rate-limiting enzyme in *de novo* pyrimidine synthesis (Figure 2F). S6K1 KO cells were similarly sensitive to inhibition of DHODH, confirming that S6K1 is not the driver of pyrimidine synthesis (Supplemental Figure 6C), suggesting that active pS6, as measured in our proteomic phenotype, is a biomarker for this mTOR-driven pyrimidine dependency.

DHODH is highly expressed in pS6+ cells

To further align active signaling and metabolic state in primary samples, we developed a CyTOF panel to capture these features in single cells and analyzed 31 primary B-ALL patient samples (Figure 2F, Supplemental Table 4-5). Using our developmental classifier[13], we observed ALL samples to be enriched in pro-BII, pre-BI, and early progenitor populations in B-ALL compared to healthy bone marrow (Pro-BII, $P = 0.00024$; Pre-BI, $P= 0.0036$; Early-non-BI, $P = 0.000352$; Supplemental Figure 8A). Developmental classification grouped by molecular subtype is shown in Supplemental Figure 8B. pS6 expression was higher in the pro-BII ($p = 0.0017$) and pre-BI populations ($p = 0.0267$), but not in early progenitors ($p > 0.999$) in leukemic cells compared to healthy BM (Supplemental Figure 8C). Proteins in the PPP (G6PD, PGD), pyrimidine synthesis (DHODH), glycolysis (ENO1, PKM2) and signaling protein pCREB were significantly overexpressed in pro-BII and/or pre-BI B-ALL cells compared to healthy BM (Figure 2G, Supplemental Figure 8C-D).

Within the patient samples, we compared expression of these proteins between pro-BII/pre-BI cells based on pS6 signaling activation (Figure 2H). pS6+ pro-BII/pre-BI cells have significantly higher expression of PGD, DHODH, and pCREB (Figure 2I-J). These results

expand our published proteomic signature of pS6+ cells[13] by defining their metabolic distinctions from healthy BM and confirmed the relationship between active pS6 signaling and pyrimidine metabolism in primary ALL cells.

Across cancer, B-ALL is most dependent on pyrimidine metabolism

Pyrimidine metabolism and DHODH have previously been implicated in acute myeloid leukemia[25-29]. To assess the dependency on pyrimidine metabolism across cancer subtypes, we evaluated the impact of DHODH knockout in the Cancer Dependency Map (DepMap.org). Among 17 types of cancer, B-ALL has the highest dependency on *DHODH* (B-ALL *vs*. all other lineages, $p < 0.001$, Figure 3A) and dependence on *de novo* pyrimidine synthesis genes (*UMPS, CAD, TYMS,* and *CTPS1*; Figure 3B; Supplemental Figure 9) compared to solid tumors.

Uridine can be synthesized *de novo* from uridine monophosphate (UMP) but can also be salvaged via uridine phosphorylase 1 (UPP1), generating ribose-1-phosphate and uracil to fuel PPP and glycolysis (Figure 3C). Analysis of Depmap data demonstrates B-ALL cell lines (n=15) had the lowest UPP1 expression among 228 hematological cell lines, suggesting minimal uridine salvage activity (Figure 3D; Supplemental Figure 10A with 31 cancer subtypes). Rescue experiments confirmed this, as ribose and uracil failed to restore pS6+ cell survival under glucose deprivation supporting PPP and glycolysis independence from uridine salvage (Figure 3E). Instead, B-ALL preferentially utilized uridine for nucleotide metabolism through its phosphorylation to UMP by uridine cytidine kinase (UCK1), reflected in a high *UCK1/UPP1* ratio (Figure 3F, Supplemental Figure 10B).

***De novo* pyrimidine synthesis is associated with poor prognosis in B-ALL**

We previously reported cells with pS6+ phenotype to be associated with relapse[13]. To investigate the relationship between *de novo* pyrimidine synthesis and relapse, we analyzed RNAseq data from standard and high-risk (MP2PRT cohort, n = 1,735[30]; TARGET cohort, n = 181) B-ALL patients. Pathway enrichment revealed that diagnostic samples from patients who experienced relapse have higher expression of genes associated with pyrimidine synthesis compared to patients who are in continuous remission ($p = 3.49e-05$, MP2PRT in Figure 4A and $p = 8.08e-08$, TARGET in Figure 4B). Furthermore, consistent with the gene signatures identified in relapse-predictive pS6+ cells, we observed increased expression of genes involved

in mitochondrial function, MYC targets, and glycolysis in the diagnostic samples from patients who experienced relapse (Supplemental Table 6).

Examining individual genes, *DHODH* expression was higher in patients who experienced relapse within the MP2PRT dataset (p = 0.025, Figure 4C) and predicted inferior event free survival (EFS) in both datasets (MP2PRT p = 0.002; TARGET p = 0.036, Figure 3E-F) and overall survival (OS) in MP2PRT dataset (p = 0.015, Supplemental Figure 11A). *UMPS* expression was significantly higher in patients who experienced relapse compared to those in continuous remission (MP2PRT p = 0.021; TARGET p = 0.008, Figure 4C-D) and correlated with worse EFS (p = 0.019) and OS (p = 0.00026, Figure 3F and Supplemental Figure 11B). These findings suggest that elevated expression of *de novo* pyrimidine synthesis genes, particularly *DHODH* and *UMPS*, are related to disease prognosis and clinical outcomes.

Active signaling predicts sensitivity to DHODH inhibition

To evaluate DHODH activity across different molecular subtypes of B-ALL, we used NetBID2 (data-driven Network-based Bayesian Inference of Drivers)[18,19] to analyze transcriptomic profiles from 1,985 B-ALL patients[20]. DHODH was predicted to be active in 54% of genomic subtypes (Figure 5A) with high activity in several subtypes of high-risk leukemia (e.g. *KMT2A* rearranged, *MEF2D*, *PAX5 P80R*, *BCL2/MYC*)[20,31]. NETBID2 analysis also revealed strong DHODH activity in more common subtypes like *DUX4*, *ETV6-RUNX1,* and *TCF3-PBX1,* with variability in Ph-like and Ph+ subtypes, suggesting metabolic heterogeneity in patients within the same molecular subtype and consistent with our single-cell proteomic data.

To validate these predictions and explore the therapeutic potential of DHODH targeting in B-ALL, we assessed the half-maximal inhibitory concentration (IC50) values of DHODH inhibitor BAY-2402234 in B-ALL cells (Figure 5B). BAY-2402234 demonstrated nanomolar potency across multiple subtypes—including *DUX4*, *TCF3-PBX1*, *ETV6-RUNX1*, *KMT2A*-rearranged, and even *TP53*-mutant near-haploid Nalm16 cells—in line with NetBID2 predictions; notably, all $pS6^+$ lines were sensitive to DHODHi (5/5, 100%) compared with only one of three $pS6^-$ lines (33.3%; Figure 5B).

We next evaluated a panel of PDXs across several molecular subtypes. Mirroring our cell line analyses (Figure 1C), we defined signaling status in each PDX sample (Figure 5C). Consistent with NetBID2 predictions and the cell line results, 7 of 14 PDXs demonstrated clear

responses to DHODHi, with the strongest effects observed in pS6+ PDXs harboring MEF2D or TCF3-PBX1 rearrangements (Figure 5D). We found a robust correlation between the strength of pS6 signaling and sensitivity to DHODHi in PDXs (n = 14, p = 0.0007, Figure 5E). Developmental classification confirmed that pro-BII and pre-BI were the predominant subpopulations in cell lines and PDXs (Supplemental Figure 12).

To identify cellular features predictive of DHODHi response, we applied XGBoost (eXtreme Gradient Boosting) binary classification[32]. pS6 and DHODH expression in pro-BII and pre-BI cells emerged as the top predictors (Figure 5F). DHODH inhibition reduced the expression of pS6, PPP protein G6PD, and glycolytic proteins ENO1 and PKM2, suggesting that BAY-2402234 preferentially targets cells with high pS6 signaling and high PPP activity, required for pyrimidine metabolism (Supplemental Figure 13A and B). In addition, we observed increased citrate synthase (CS) expression and mitochondrial mass following BAY-2402234 treatment in 3 cell lines (Supplemental Figure 13C and D), suggesting post-treatment metabolic shift towards OXPHOS following DHODHi. We confirmed that DHODHi selectively targets pS6+ cells over time in Nalm16 and SJ45503 cells (Figure 5G). These data demonstrate pS6 signaling is a surrogate marker for pyrimidine dependency in B-ALL.

To investigate whether active pS6 signaling predicts sensitivity to DHODHi in other hematologic malignancies, we analyzed 12 additional cell lines including 5 T-ALL, 3 myeloid leukemias, and 4 B-cell lymphomas representing a range of pS6 activity levels and variable responses to BAY-2402234 (Supplemental Figure 14A-B). Among these cell lines, B- and T-ALL have higher DHODH protein expression and lower UPP1 mRNA expression than myeloid leukemia and B-cell lymphomas (Supplemental Figure 14C-D). T-ALL and myeloid leukemia cells with low UPP1 and high pS6 expression demonstrated sensitivity to DHODHi, whereas B-cell lymphomas were largely insensitive regardless of UPP1/pS6 status (Supplemental Figure 14E). These findings extend the relevance of our observations to additional hematologic malignancies including other types of acute leukemia.

Uridine concentrations in human serum range from 1–10 μM. Because physiologic uridine was reported to blunt DHODH inhibitor activity in lung cancer[33], we directly tested whether clinically relevant uridine levels interfere with DHODHi efficacy in ALL. Eight ALL cell lines were treated with BAY-2402234 while titrating uridine across 0–30 μM. In DHODHi-sensitive lines, 3–10 μM uridine produced no or minimal attenuation of cytotoxicity, and full

rescue required ≥30 μM. Less sensitive lines showed partial, but not complete, rescue at 3–10 μM (Supplemental Figure 15). Thus, DHODH inhibition remains effective with physiologic uridine concentrations, supporting the translational relevance of BAY-2402234 as a therapeutic approach in ALL.

DHODH inhibition prolongs survival in pS6+ B-ALL xenograft models

Given that pS6 signaling strength predicts the *in vitro* sensitivity to DHODHi, we assessed the *in vivo* efficacy of BAY-2402234 in B-ALL PDX (SJ18305, SJ45503) and cell lines (Nalm6, Nalm16) xenografts. NSG mice received vehicle or BAY-2402234 (5 mg/kg) five times per week for 24 doses (Figure 6A, Supplemental Figure 16A). Treatment was well-tolerated (Supplemental Figure 16B).

DHODHi significantly slowed tumor progression compared to vehicle in pS6+ samples ($p < 0.0001$ in SJ18305, Nalm16 and Nalm6; Figures. 6B-E and Supplemental Figure 16C). By contrast, DHODHi did not slow disease progression in SJ45503, which possessed low pS6 signaling strength (Figure 6F). In SJ18305, DHODHi significantly reduced leukemia burden within the BM ($p = 0.0139$, Figure 6G) and spleen ($p = 0.007$, Figure 6H). Survival analysis demonstrated that DHODHi significantly prolonged survival in all pS6+ xenograft models, regardless of pS6 activity (SJ18305 $p = 0.0016$; Nalm16 $p = 0.0047$; Nalm6 $p = 0.0031$; Figure 6I-J, Supplemental Figure 16D), demonstrating a modest survival benefit in the SJ45503 mice as compared to vehicle ($p = 0.028$, Supplemental Figure 16E). Consistent with the in vitro findings, cells from the experimental endpoint in the Nalm16-derived xenografts exhibited a marked reduction in pS6, ENO1, PKM2, G6PD, and PGD levels and an increase in CS expression (Supplemental Figure 16F-H). Together, these findings highlight DHODH inhibition as a promising therapy for B-ALL, with potential benefit even in cases with moderate pS6 activation.

Discussion

Relapsed and refractory B-ALL remains a significant clinical challenge. Previous studies have independently associated the activation of B-cell developmental signaling pathways and increased glucose consumption with chemo-resistance and relapse risk[13,34-38]. However, these paradigms have not been previously linked. Here, we demonstrate activated signaling, reflected by activation of pS6 as a surrogate biomarker, drives glucose utilization into PPP and *de novo* pyrimidine synthesis, revealing a novel pyrimidine dependency in B-ALL. DHODH is essential

for this process and broadly active in most B-ALL molecular subtypes, including high-risk leukemias. DHODHi demonstrated remarkable efficacy *in vitro* and *in vivo*. Sensitivity to DHODHi correlated with pS6 signaling strength, identifying pS6 as a biomarker of pyrimidine dependency. These findings suggest targeting DHODH is a promising strategy for B-ALL.

During normal B-cell development, IL-7R signaling drives pro-B cell proliferation, whereas pre-BCR signaling activates RAS and mTOR pathways during pre-B cell maturation[14]. Sustained activation of these pathways is associated with chemo-resistance and relapse in B-ALL, particularly high-risk subtypes such as Ph-like and Ph+ B-ALL[15-17]. Activation of SYK, a proximal member of the pre-BCR and PI3K/mTOR signaling pathways, is also implicated in chemo-resistance in TCF3-PBX1 and KMT2A-rearranged B-ALL[39-41]. We previously showed that activation of these pathways predicts relapse after chemotherapy and supports glucocorticoid resistance[13,37]. However, RAS, PI3K, and mTOR inhibitors has shown limited clinical efficacy, apart from BCR-ABL rearranged (Ph+) B-ALL[42], partly due to resistance mechanisms such as activation of parallel signaling pathways[43-45]. Upstream signaling may converge on mTORC1 as a common downstream molecule which then regulates S6 kinases to drive *de novo* pyrimidine synthesis via CAD phosphorylation[23,24]. Our data show that pS6+ cells have increased CAD phosphorylation, which TKIs effectively suppress. CAD catalyzes the initial steps in the *de novo* pyrimidine synthesis pathway, followed by DHODH, which catalyzes the rate-limiting step. Consistent with this, inhibition of mTOR makes B-ALL resistant to DHODH inhibition while KO of S6K1 does not. Thus, we propose that directly targeting *de novo* pyrimidine synthesis through DHODH inhibition overcomes the challenges of TKI resistance by hitting the convergence of several signaling pathways.

B-cell oncogenic signaling and transcription factor dysregulation drive metabolic adaptations favoring transformation[46]. Tumor suppressors like PAX5 and IKAROS regulate glucose metabolism, and high glucose availability correlates with chemo-resistance and poor outcomes[35,47,48]. Further, in line with our data, B-ALL cells divert glucose-derived carbons toward the PPP[49]. Our results support these observations and continue to implicate these pathways in resistance to chemotherapy and relapsed disease.

Since Sidney Farber introduced anti-folates in childhood leukemia treatment over 70 years ago[50], targeting nucleotide synthesis has been part of therapeutic backbones for ALL. However, pyrimidines have not been specifically targeted. While DHODH inhibitors have been

approved as immunomodulatory agents, their therapeutic potential in cancer is emerging[51-55]. In hematologic malignancies, it has been explored in preclinical settings in AML[25-29], B-cell lymphoma[56,57], and T-ALL[58,59], but clinical trials in AML have not progressed due to lack of efficacy (NCT03404726). Our data identify B-ALL as the most DHODH-dependent cancer type, showing minimal uridine salvage activity due to low UPP1 expression, unlike pancreatic cancer and AML, where salvage pathways fuel PPP and glycolysis[60,61], Gene expression analysis of 1,985 B-ALL patients showed pyrimidine dependency in most B-ALL genetic subtypes, including high-risk leukemias patients with KMT2A-rearranged, PAX5 P80R, BCL2/MYC[20,31,62]. Consistent with this, DHODHi was detrimental in several *in vitro* and *in vivo* standard-risk and high-risk leukemia models. Our data showed increased citrate synthase expression and elevated mitochondrial mass upon DHODH inhibition, consistent with prior findings in T-ALL[58], demonstrating upregulation of electron transport chain genes to maintain ATP production. This is notable since DHODH resides at the mitochondrial inner membrane, acting as part of the electron transport chain[63,64]. These results suggest that cells attempt to further activate OXPHOS to compensate for DHODH inhibition.

In conclusion, B-ALL cells with active mTOR signaling exhibit increased reliance on *de novo* pyrimidine synthesis. DHODH inhibition disrupts this metabolic dependency and demonstrates potent in vitro and in vivo efficacy, defining a targetable metabolic vulnerability and a potential therapeutic strategy for B-ALL.

Data availability

CyTOF data from clinically annotated patient samples, cell lines, and PDX samples are available in Community Cytobank (https://community.cytobank.org) under accession numbers 119315 (patients), 119316 (cell lines), 119640, and 119641 (PDX samples) respectively.

Bulk RNA-seq data from primary samples in our previously published patient cohort (n=6) have been deposited in NCBI Gene Expression Omnibus (GEO) and are accessible through GEO accession number GSE286115.

The TARGET dataset used for this study is accessible through the TARGET website at https://ocg.cancer.gov/programs/target/data-matrix. TARGET BAM and FASTQ sequence files are accessible through the database of genotypes and phenotypes (dbGaP; https://www.ncbi.nlm.nih.gov/projects/gap/cgi-bin/study.cgi?study_id=phs000218.v24.p8) under

accession no. phs000218 (TARGET) and at NCI's Genomic Data Commons (http://gdc.cancer.gov) under project TARGET. Transcriptomic data in MP2PRT dataset are accessible in dbGaP: Project ID: MP2PRT-ALL; accession number: phs002005.v1.p1 (https://www.ncbi.nlm.nih.gov/projects/gap/cgi-bin/dataset.cgi?study_id=phs002005.v1.p1).

Acknowledgments

We would like to thank current and past members of the Davis laboratory for helpful discussions. This work was supported by the National Institutes of Health R01-CA251858 and the Stanford Maternal Child Health Research Institute, MCHRI, and Alex's Lemonade Stand Foundation. Y.L. is supported by R01-CA251858 and MCHRI. J.S. is supported by Associazione Italiana per la Ricerca sul Cancro (AIRC; grant no. 27325). K.L.D is supported by the Anne T. and Robert M. Bass Endowed Faculty Scholar in Pediatric Cancer and Blood Disease and the Harriet and Mary Zelencik Endowment. We acknowledge the PROPEL project at St. Jude for contribution of annotated PDX expanded ALL cells.

Author contributions

Y.L. conceived of, designed, and led this study, designed and performed experiments, analyzed and interpreted data, generated the figures, and wrote the manuscript. H.J. conducted experiments and analyzed stable isotope metabolomics data. J.L. performed data analysis for the TARGET and MP2PRT datasets. L.S., A.J., and D.J. contributed to CyTOF experiments and validated the antibody panel used in these experiments. M.M. and C.P. assisted with *in vivo* mouse studies, cell culture work, retrovirus generation and transduction. A.K. performed the CyTOF data analysis using XGboost. T.C. provided guidance for MP2PRT dataset analysis. P.D. and J.S. performed cell sorting, RNA extraction and performed RNA-seq data analysis. J.M., I.I., Q.G. assisted in genomic analyses. T.K. contributed to developmental classification data analysis using tidytof. A.W. contributed to western blot analysis. F.H. and S.B. provided guidance on CyTOF experiments. M.H., N.J.L, K.M.S., C.G.M., M.L., R.H, C.F., J.Yu. and J.Yang. contributed patient or PDX samples and provided clinical data. H.J., J.L., L.S., P.D., J.Yu., J.Yang. and J.Ye. provided guidance and scientific input. K.L.D. conceived of and designed this study, provided guidance and scientific input, interpreted data, and wrote the manuscript. All authors discussed the results and prepared the manuscript.

446

447 **Conflict of Interest Disclosures**

448 The authors declare no potential conflicts of interest.

449

450

451

References

1. Hanahan D, Weinberg RA. Hallmarks of cancer: the next generation. *Cell*. 2011;144(5):646-674.
2. Jones CL, Inguva A, Jordan CT. Targeting Energy Metabolism in Cancer Stem Cells: Progress and Challenges in Leukemia and Solid Tumors. *Cell Stem Cell*. 2021;28(3):378-393.
3. Mishra SK, Millman SE, Zhang L. Metabolism in acute myeloid leukemia: mechanistic insights and therapeutic targets. *Blood*. 2023;141(10):1119-1135.
4. DeBerardinis RJ, Chandel NS. We need to talk about the Warburg effect. *Nature Metabolism*. 2020;2(2):127-129.
5. De Carli E, Wang X, Puget S. IDH1 and IDH2 mutations in gliomas. *N Engl J Med*. 2009;360(21):2248; author reply 2249.
6. Mardis ER, Ding L, Dooling DJ, et al. Recurring mutations found by sequencing an acute myeloid leukemia genome. *N Engl J Med*. 2009;361(11):1058-1066.
7. Amatangelo MD, Quek L, Shih A, et al. Enasidenib induces acute myeloid leukemia cell differentiation to promote clinical response. *Blood*. 2017;130(6):732-741.
8. Yen K, Travins J, Wang F, et al. AG-221, a First-in-Class Therapy Targeting Acute Myeloid Leukemia Harboring Oncogenic IDH2 Mutations. *Cancer Discov*. 2017;7(5):478-493.
9. Wang F, Travins J, DeLaBarre B, et al. Targeted inhibition of mutant IDH2 in leukemia cells induces cellular differentiation. *Science*. 2013;340(6132):622-626.
10. Miller KD, Nogueira L, Mariotto AB, et al. Cancer treatment and survivorship statistics, 2019. *CA Cancer J Clin*. 2019;69(5):363-385.
11. Siegel DA, Henley SJ, Li J, Pollack LA, Van Dyne EA, White A. Rates and Trends of Pediatric Acute Lymphoblastic Leukemia - United States, 2001-2014. *MMWR Morb Mortal Wkly Rep*. 2017;66(36):950-954.
12. Rheingold SR, Bhojwani D, Ji L, et al. Determinants of survival after first relapse of acute lymphoblastic leukemia: a Children's Oncology Group study. *Leukemia*. 2024.
13. Good Z, Sarno J, Jager A, et al. Single-cell developmental classification of B cell precursor acute lymphoblastic leukemia at diagnosis reveals predictors of relapse. *Nat Med*. 2018;24(4):474-483.
14. Rickert RC. New insights into pre-BCR and BCR signalling with relevance to B cell malignancies. *Nat Rev Immunol*. 2013;13(8):578-591.
15. Irving J, Matheson E, Minto L, et al. Ras pathway mutations are prevalent in relapsed childhood acute lymphoblastic leukemia and confer sensitivity to MEK inhibition. *Blood*. 2014;124(23):3420-3430.
16. Shaw AC, Swat W, Ferrini R, Davidson L, Alt FW. Activated Ras signals developmental progression of recombinase-activating gene (RAG)-deficient pro-B lymphocytes. *J Exp Med*. 1999;189(1):123-129.
17. Feldhahn N, Klein F, Mooster JL, et al. Mimicry of a constitutively active pre-B cell receptor in acute lymphoblastic leukemia cells. *J Exp Med*. 2005;201(11):1837-1852.
18. Dong X, Ding L, Thrasher A, et al. NetBID2 provides comprehensive hidden driver analysis. *Nat Commun*. 2023;14(1):2581.
19. Du X, Wen J, Wang Y, et al. Hippo/Mst signalling couples metabolic state and immune function of CD8alpha(+) dendritic cells. *Nature*. 2018;558(7708):141-145.
20. Gu Z, Churchman ML, Roberts KG, et al. PAX5-driven subtypes of B-progenitor acute lymphoblastic leukemia. *Nat Genet*. 2019;51(2):296-307.

21. Yin C, Qie S, Sang N. Carbon source metabolism and its regulation in cancer cells. *Crit Rev Eukaryot Gene Expr*. 2012;22(1):17-35.
22. Jiang H, Greathouse RL, Tiche SJ, et al. Mitochondrial Uncoupling Induces Epigenome Remodeling and Promotes Differentiation in Neuroblastoma. *Cancer Res*. 2023;83(2):181-194.
23. Robitaille AM, Christen S, Shimobayashi M, et al. Quantitative phosphoproteomics reveal mTORC1 activates de novo pyrimidine synthesis. *Science*. 2013;339(6125):1320-1323.
24. Ben-Sahra I, Howell JJ, Asara JM, Manning BD. Stimulation of de novo pyrimidine synthesis by growth signaling through mTOR and S6K1. *Science*. 2013;339(6125):1323-1328.
25. Sykes DB, Kfoury YS, Mercier FE, et al. Inhibition of Dihydroorotate Dehydrogenase Overcomes Differentiation Blockade in Acute Myeloid Leukemia. *Cell*. 2016;167(1):171-186 e115.
26. So J, Lewis AC, Smith LK, et al. Inhibition of pyrimidine biosynthesis targets protein translation in acute myeloid leukemia. *EMBO Mol Med*. 2022;14(7):e15203.
27. Cao L, Weetall M, Trotta C, et al. Targeting of Hematologic Malignancies with PTC299, A Novel Potent Inhibitor of Dihydroorotate Dehydrogenase with Favorable Pharmaceutical Properties. *Mol Cancer Ther*. 2019;18(1):3-16.
28. Christian S, Merz C, Evans L, et al. The novel dihydroorotate dehydrogenase (DHODH) inhibitor BAY 2402234 triggers differentiation and is effective in the treatment of myeloid malignancies. *Leukemia*. 2019;33(10):2403-2415.
29. Zhou J, Yiying Quah J, Ng Y, et al. ASLAN003, a potent dihydroorotate dehydrogenase inhibitor for differentiation of acute myeloid leukemia. *Haematologica*. 2020;105(9):2286-2297.
30. Chang TC, Chen W, Qu C, et al. Genomic Determinants of Outcome in Acute Lymphoblastic Leukemia. *J Clin Oncol*. 2024:JCO2302238.
31. Paietta E, Roberts KG, Wang V, et al. Molecular classification improves risk assessment in adult BCR-ABL1-negative B-ALL. *Blood*. 2021;138(11):948-958.
32. Chen TQ, Guestrin C. XGBoost: A Scalable Tree Boosting System. *Kdd'16: Proceedings of the 22nd Acm Sigkdd International Conference on Knowledge Discovery and Data Mining*. 2016:785-794.
33. Abbott KL, Ali A, Casalena D, et al. Screening in serum-derived medium reveals differential response to compounds targeting metabolism. *Cell Chem Biol*. 2023;30(9):1156-1168 e1157.
34. Tremblay CS, Saw J, Boyle JA, et al. STAT5 activation promotes progression and chemotherapy resistance in early T-cell precursor acute lymphoblastic leukemia. *Blood*. 2023;142(3):274-289.
35. Hulleman E, Kazemier KM, Holleman A, et al. Inhibition of glycolysis modulates prednisolone resistance in acute lymphoblastic leukemia cells. *Blood*. 2009;113(9):2014-2021.
36. Kim JM, Fang J, Rheingold S, Aplenc R, Wasserman R, Grupp SA. Cytoplasmic micro heavy chain confers sensitivity to dexamethasone-induced apoptosis in early B-lineage acute lymphoblastic leukemia. *Cancer Res*. 2002;62(15):4212-4216.
37. Sarno J, Domizi P, Liu Y, et al. Dasatinib overcomes glucocorticoid resistance in B-cell acute lymphoblastic leukemia. *Nat Commun*. 2023;14(1):2935.
38. Orgel E, Framson C, Buxton R, et al. Caloric and nutrient restriction to augment chemotherapy efficacy for acute lymphoblastic leukemia: the IDEAL trial. *Blood Adv*. 2021;5(7):1853-1861.

39. Uckun FM, Qazi S. Tyrosine kinases in KMT2A/MLL-rearranged acute leukemias as potential therapeutic targets to overcome cancer drug resistance. *Cancer Drug Resist*. 2022;5(4):902-916.
40. Loftus JP, Yahiaoui A, Brown PA, et al. Combinatorial efficacy of entospletinib and chemotherapy in patient-derived xenograft models of infant acute lymphoblastic leukemia. *Haematologica*. 2021;106(4):1067-1078.
41. Geng H, Hurtz C, Lenz KB, et al. Self-enforcing feedback activation between BCL6 and pre-B cell receptor signaling defines a distinct subtype of acute lymphoblastic leukemia. *Cancer Cell*. 2015;27(3):409-425.
42. Tasian SK, Silverman LB, Whitlock JA, et al. Temsirolimus combined with cyclophosphamide and etoposide for pediatric patients with relapsed/refractory acute lymphoblastic leukemia: a Therapeutic Advances in Childhood Leukemia Consortium trial (TACL 2014-001). *Haematologica*. 2022;107(10):2295-2303.
43. Quentmeier H, Eberth S, Romani J, Zaborski M, Drexler HG. BCR-ABL1-independent PI3Kinase activation causing imatinib-resistance. *J Hematol Oncol*. 2011;4:6.
44. Duy C, Hurtz C, Shojaee S, et al. BCL6 enables Ph+ acute lymphoblastic leukaemia cells to survive BCR-ABL1 kinase inhibition. *Nature*. 2011;473(7347):384-388.
45. Vo TT, Lee JS, Nguyen D, et al. mTORC1 Inhibition Induces Resistance to Methotrexate and 6-Mercaptopurine in Ph(+) and Ph-like B-ALL. *Mol Cancer Ther*. 2017;16(9):1942-1953.
46. Muschen M. Metabolic gatekeepers to safeguard against autoimmunity and oncogenic B cell transformation. *Nat Rev Immunol*. 2019;19(5):337-348.
47. Chan LN, Chen Z, Braas D, et al. Metabolic gatekeeper function of B-lymphoid transcription factors. *Nature*. 2017;542(7642):479-483.
48. Pan L, Hong C, Chan LN, et al. PON2 subverts metabolic gatekeeper functions in B cells to promote leukemogenesis. *Proc Natl Acad Sci U S A*. 2021;118(7).
49. Xiao G, Chan LN, Klemm L, et al. B-Cell-Specific Diversion of Glucose Carbon Utilization Reveals a Unique Vulnerability in B Cell Malignancies. *Cell*. 2018;173(2):470-484 e418.
50. Farber S, Diamond LK. Temporary remissions in acute leukemia in children produced by folic acid antagonist, 4-aminopteroyl-glutamic acid. *N Engl J Med*. 1948;238(23):787-793.
51. Koundinya M, Sudhalter J, Courjaud A, et al. Dependence on the Pyrimidine Biosynthetic Enzyme DHODH Is a Synthetic Lethal Vulnerability in Mutant KRAS-Driven Cancers. *Cell Chem Biol*. 2018;25(6):705-717 e711.
52. Shi DD, Savani MR, Levitt MM, et al. De novo pyrimidine synthesis is a targetable vulnerability in IDH mutant glioma. *Cancer Cell*. 2022;40(9):939-956 e916.
53. Olsen TK, Dyberg C, Embaie BT, et al. DHODH is an independent prognostic marker and potent therapeutic target in neuroblastoma. *JCI Insight*. 2022;7(17).
54. Pal S, Kaplan JP, Nguyen H, et al. A druggable addiction to de novo pyrimidine biosynthesis in diffuse midline glioma. *Cancer Cell*. 2022;40(9):957-972 e910.
55. Gwynne WD, Suk Y, Custers S, et al. Cancer-selective metabolic vulnerabilities in MYC-amplified medulloblastoma. *Cancer Cell*. 2022;40(12):1488-1502 e1487.
56. McDonald G, Chubukov V, Coco J, et al. Selective Vulnerability to Pyrimidine Starvation in Hematologic Malignancies Revealed by AG-636, a Novel Clinical-Stage Inhibitor of Dihydroorotate Dehydrogenase. *Mol Cancer Ther*. 2020;19(12):2502-2515.

57. Eriksen-Gjerstad M, Tveit Karlsen I, Fandalyuk Z, et al. Dihydroorotate dehydrogenase inhibition acts synergistically with tyrosine kinase inhibitors to induce apoptosis of mantle cell lymphoma cells. *EJHaem*. 2022;3(3):913-918.
58. Sexauer AN, Alexe G, Gustafsson K, et al. DHODH: a promising target in the treatment of T-cell acute lymphoblastic leukemia. *Blood Adv*. 2023;7(21):6685-6701.
59. Yang L, Ma D, Liu S, Zou L. The DHODH inhibitor teriflunomide impedes cell proliferation and enhances chemosensitivity to daunorubicin (DNR) in T-cell acute lymphoblastic leukemia. *Ann Hematol*. 2024.
60. Skinner OS, Blanco-Fernandez J, Goodman RP, et al. Salvage of ribose from uridine or RNA supports glycolysis in nutrient-limited conditions. *Nat Metab*. 2023;5(5):765-776.
61. Nwosu ZC, Ward MH, Sajjakulnukit P, et al. Uridine-derived ribose fuels glucose-restricted pancreatic cancer. *Nature*. 2023;618(7963):151-158.
62. Winters AC, Bernt KM. MLL-Rearranged Leukemias-An Update on Science and Clinical Approaches. *Front Pediatr*. 2017;5:4.
63. Zhou Y, Tao L, Zhou X, et al. DHODH and cancer: promising prospects to be explored. *Cancer Metab*. 2021;9(1):22.
64. Fang J, Uchiumi T, Yagi M, et al. Dihydro-orotate dehydrogenase is physically associated with the respiratory complex and its loss leads to mitochondrial dysfunction. *Biosci Rep*. 2013;33(2):e00021.

Figure 1. pS6+ cells have distinct metabolic gene signatures and are glucose dependent

A. Whole transcriptome sequencing was performed in primary diagnostic BM samples from known pS6+ patients who would go on relapse (n=3) and pS6- patients who remain in continued remission (n=3).

B. Differential expression analysis between primary pS6+ and pS6- cells. Gene set enrichment analysis (GSEA) was performed with the Hallmark database (FDR < 0.05). Diagnostic pS6+ cells are enriched for genes in PI3K and mTOR pathways (blue) as well as several metabolic pathways (red).

C. Z-score based on frequency of cells positive for phosphorylated S6, AKT, ERK, 4EBP1 and CREB in B-ALL cell lines in basal state defines pS6+ lines (n=6, Nalm6, RCH-ACV, 697, Kasumi2, Nalm16 and REH) and pS6- lines (n=3, RS4;11, Nalm20, MHH-CALL-4).

D. Expression (arcsinh transformed mean) of pS6 (S235/236), pAKT (S273), pERK (T202/Y204) and pCREB (S133) in pS6+ and pS6- cell lines (pS6, p = 0.002; pERK, p = 0.004; pAKT, p = 0.095, ns; p4EBP1, p = 0.095, ns; pCREB, p = 0.095, ns).

E. Extracellular acidification rate (ECAR) indicating glycolytic activity in pS6+ cell lines (red) compared to pS6- cell lines (black; p = 0.0039).

F. Correlation between the frequency of pS6+ cells and the glycolytic activity (measured by ECAR) in B-ALL cell lines (n=9, p = 0.021, $R^2 = 0.56$). Each dot represents individual cell line colored by pS6 relative expression level (z-score of arcsinh transformed mean value) measured by CyTOF.

G. Cell viability after culture in medium with or without glucose (open bar) for 48 hours in pS6+ cells (red, n = 5) and pS6- cells (gray, n = 3). Cell death is measured by annexin V and PI staining by flow cytometry. Nalm6 p = 0.00098; 697 p = 0.0064; Kasumi2 p = 0.0022; Nalm16 p = 0.026; REH p = 0.0183; RS4;11, p = 0.614; MHH-CALL-4 p = 0.523; Nalm20 p = 0.081. Three or four biological replicates were performed.

All data in dot plots and bar graphs are mean ± SD. Statistical tests used were Welch's t test followed by Holm-Sidak multiple comparison test (D); Welch's t test (E, I); and multiple paired t test followed using Šídák-Bonferroni method (G). ns, not significant, *p < 0.05, **p < 0.01, ***p < 0.001.

Figure 2. PI3K/mTOR signaling drives glucose-dependent pyrimidine synthesis in B-ALL cells

A. Schematic of $^{13}C_6$ glucose tracing to illustrate glucose flow through glycolysis, PPP and purine/pyrimidine synthesis. *De novo* synthesis converts phosphoribosyl pyrophosphate (PRPP) into uridine monophosphate (UMP) or inosine monophosphate (IMP), while the salvage pathway recycles nucleosides and nucleobases into nucleoside 5′-monophosphates (NMPs) or deoxy NMPs in one adenosine triphosphate (ATP)- or PRPP-dependent step. Pyrimidine synthesis pathways are highlighted: red for *de novo*, blue for salvage. Key enzymes include CAD (carbamoyl phosphate synthetase II, aspartate transcarbamoylase and dihydroorotase), CTPS1 (CTP synthase 1), DHODH (dihydroorotate dehydrogenase), TS (thymidylate synthase), UCK1/2

(uridine–cytidine kinases 1 and 2), UMPS (UMP synthase); UPP1 (uridine phosphorylase 1). The figure was created in Biorender.

B. Fractional labeling of m+5 glucose carbons in PPP products: UDP (uridine diphosphate, p = 0.0233); UTP (uridine triphosphate, p =0.002) and ATP (adenosine triphosphate, p =0.0342) in glutamine deprived conditions in pS6+ and pS6- cell lines.

C. Cell viability after glucose deprivation (GD) for 48 hours with and without supplementation of various metabolites: uridine (1mM), pyruvate (5mM), aspartate (5mM), pyrimidine (1mM) and purine (1mM). Analyses included pS6+ cell lines (n = 5) and pS6- cell lines (n = 3).

D. Pathway of carbamoyl phosphate synthetase (CAD) phosphorylation (left panel). Western blot of pCAD (S1859), pS6 (S235/S236), total CAD, total ribosomal protein S6 and GAPDH (as loading control) in pS6+ (Nalm6, 697, Nalm16, in red) and pS6- (RS4;11, Nalm20, MHH-CALL4, in black) cell lines. Band intensities were analyzed by Image J software and normalized to first lane and loading control as indicated under each lane.

E, Western blot of pCAD (S1859), pS6 (S235/S236), total CAD, total ribosomal protein S6 and GAPDH (as loading control) in B-ALL cell line Nalm6 and PDX sample (SJ18305) in the presence or absence of tyrosine kinase inhibitors targeting kinases in the PI3K/mTOR pathway. S6K1 (PF-4708671: 10, 20μM) PI3K (LY294002: 10, 20μM), mTOR (rapamycin: 2.5, 5μM), SYK (PRT062607 HCl: 2.5, 5μM) for 24 hours.

F. CyTOF panel utilized to evaluate expression of glycolysis, PPP, and pyrimidine synthesis proteins along with signaling molecules in primary cells. Measured proteins are in color, non-measured proteins are in gray. The figure was created in Biorender.

G. Median expression of metabolic and signaling proteins between cell populations and primary B-ALL BM cells from diagnosis (n = 31) and healthy BM (n = 5) in the Pro-BII and Pre-BI population as profiled by CyTOF. Leukemia cells were classified into their developmental state using our developmental classifier (see Supplemental Methods and Supplemental Figure 7).

H. Gating strategy defining pS6+ and pS6- cells in patient samples profiled by CyTOF; pS6+ cells were defined as events with pS6 counts > 10.

I. PGD (x-axis), DHODH (y-axis) and pCREB (color scale) expression between $pS6^{+}$ (left) and $pS6^{-}$ (right) cell populations as gated in 'H'.

J. Median expression values of DHODH, PGD and pCREB measured by CyTOF across two populations: pS6+ (red bar) and pS6– cells (black bar) in Pro-BII/Pre-BI cells from B-ALL patient samples (n=31). Each gray line links the two measurements (pS6+ vs. pS6−) for the same sample.

Data are displayed as mean ± SD. Statistical test used to compare ^{13}C labelling fraction between pS6+ and pS6- cells is Welch t test (B). Two-way ANOVA followed by Šidák's multiple comparisons test was used to compare the rescue effect of metabolites from glucose deprivation (C). Multiple unpaired *t*-test was used to compare protein median expression in leukemia samples and healthy BMs (G). Multiple paired *t*-test followed by Šídák-Bonferroni correction

was used to compare protein median expression in pS6+ and – population in patient samples (J). *p < 0.05, **p < 0.01, ***p < 0.001.

Figure 3. Across cancer, B-ALL is most dependent on pyrimidine metabolism.

A. Effect of DHODH KO in cell lines across cancer subtypes in genome-wide CRISPR screens (DepMap 22Q2 Public+Score, Chronos). B-ALL (in red) is the most dependent on DHODH for growth and survival among 17 types of cancer. The x-axis shows cancer types of cell lines. The y-axis shows the DHODH dependency score (gene effect) per cell line. Commonly essential genes exhibit a median Chronos score of −1 as indicated (dashed line).

B. Comparison of dependencies in B-cell leukemia (B-ALL) vs solid tumors. The x-axis displays the difference in average CRISPR score per gene between B-ALL and solid tumors, while the y-axis represents significance using -log10(p-value). Purple dots represent "dependency" genes that are preferentially dependent in B-ALL compared to solid tumors. Their loss is more detrimental to B-ALL cells than to solid tumor cells. Blue dots show "tolerance" genes that are not essential in B-ALL. A series of genes involved in pyrimidine synthesis (*DHODH*, *UMPS*, *CAD*, *TYMS* and *CTPS1, red*) are among the most essential genes in B-ALL.

C. Schematic figure to show that uridine can be synthesized from orotate and PRPP in *de novo* synthesis pathway indicated as red arrows and salvaged from cytidine indicated as blue arrows. Other studies have shown that uridine can be converted to uracil and ribose-1P to fuel PPP and glycolysis. The figure was created in Biorender.

D. Gene expression of UPP1 (encoding uridine phosphorylase, a pyrimidine salvage enzyme that catalyzes the reversible phosphorylation of uridine to uracil and ribose-1-phosphate) in 229 cell lines from 12 different subtypes of hematological malignancies in Depmap RNA-seq data (Batch Corrected Expression Public 24Q2). B-ALL cell lines (marked in red) have the lowest expression of UPP1 crossing all cancer types. CML, chronic myeloid leukemia; BL, Burkitt lymphoma; AML, acute myeloid leukemia; MCL, mantle cell lymphoma; HL, Hodgkin lymphoma; ALCL, Anaplastic Large-Cell Lymphoma; T-ALL, T cell lymphoblastic leukemia/lymphoma.

E. Cell viability after glucose deprivation (GD) for 48 hours with and without rescuing by uridine (2mM), ribose (10mM) or uracil (2mM). pS6+ cells are rescued by uridine or ribose supplementations in the face of glucose deprivation. Cell apoptosis is measured by annexin V and PI staining in flow cytometry. Annexin V and PI double negative cells are live cells.

F. Ratio of gene expression of UCK1 (uridine cytidine kinase 1) to UPP1 in 229 cell lines from 12 different hematological malignancies. B-ALL cell lines ranked highest (red).

Data in box-whisker plot (A) are shown as median value with the range of values from 10^{th} to 90^{th} percentiles. The dots above or below the lines are outliers. Data in the box-and-whisker graphs (D,F) was presented with all the data points with the line indicating median value. One way ANOVA test followed by the Holm-Šidák method for multiple comparison correction was

used to compare B-ALL with every other cancer type. Data in bar graph (E) is displayed as mean ± SD in triplicates. Two-way ANOVA followed by Šidák's multiple comparisons test was used to evaluate the rescue effect of different metabolites compared to glucose deprivation (ns, not significant, *p < 0.05, **p < 0.01, ***p < 0.001, ***p < 0.0001).

Figure 4. *De novo* pyrimidine synthesis is a metabolic vulnerability in B-ALL

A. GSEA for KEGG_pyrimidine_metabolism signature between relapsed (n=426) vs non-relapsed (n=1039) patients in the MP2PRT dataset. Enrichment score 0.489, Kolmogorov–Smirnov (KS) test of rank distribution p =3.49e-05.

B. GSEA for KEGG pyrimidine metabolism signature between relapsed (n=112) vs non-relapsed (n=75) patients with B-ALL in the NCI TARGET dataset. Enrichment score 0.354, KS test of rank distribution p =8.08e-08.

C. *DHODH* and *UMPS* relative expression in relapsed (n=426) vs non-relapsed (n=1039) patients from MP2PRT dataset (*DHODH*, P=0.025; *UMPS*, p = 0.021). The line indicates mean value.

D. *DHODH* and *UMPS* relative expression in the diagnostic samples from relapsed (n=112) vs non-relapsed (n=75) patients from NCI TARGET dataset (*DHODH* p =0.133; *UMPS* p = 0.008). The line indicates mean value.

E. Event-free survival (EFS) based on *DHODH* and *UMPS* expression in MP2PRT dataset when comparing top 10 percentile (N= 147) versus lowest 90% (n=1,318) MP2PRT, Molecular Profiling to Predict Responses to Therapy. Significance determined by Cox regression; *DHODH* p = 0.002; p = 0.214.

F. EFS based on *DHODH* and *UMPS* expression in the NCI TARGET dataset when comparing the highest quartile (n = 46) to the lowest quartiles (n = 135) Significance determined by Cox regression; DHODH p = 0.036; UMPS p = 0.019.

The Kolmogorov–Smirnov test was applied to determine whether the rank distributions of these pathways were statistically different between diagnostic samples from patients who would relapse and patients who are in remission (A, B). Statistical test between relapse vs none was Welch's *t*-test (C, D). *p < 0.05, **p < 0.01, ***p < 0.001.

Figure 5. **Active signaling predicts sensitivity to DHODH inhibition**

A. DHODH activity in 1985 molecularly defined B-ALL cases. Bold indicates subtypes tested for DHODH inhibition (DHODHi) sensitivity in vitro.

B. In vitro killing after treatment with DHODHi BAY-2402234 in cell lines (n=9). Cells were treated with increasing concentrations of BAY-2402234 for 48 hours. Apoptosis was measured by flow cytometry with Annexin V/7AAD staining. pS6+ magnitude is indicated by color with red/orange representing highest pS6 magnitude (n=5) while pS6- cells (n=3) are indicated in gray.

C. Z-score based on the median expression of signaling molecules pS6, pERK, pAKT, p4EBP1 and pCREB in Pro-BII and Pre-BI cells from PDX samples (n=17). Phospho-protein profiles were measured in CyTOF and each cell was classified by developmental classification. We defined cell lines and PDXs with pS6 median expression values (arcsinh transformed) greater than 3 as pS6+ and those no greater than 3 as pS6-. pS6+ PDXs are shown in red, while pS6- PDXs are in black. PDXs marked in bold were used for DHODHi treatment in panel D.

D. In vitro killing after treatment with BAY-2402234 in PDX samples (n=14). Cells were treated with increasing concentrations of BAY-2402234 for 72 hours. Cell viability was measured by CellTiter-Glo assay. Curves were color-coded by z-score of pS6 median value measured by CyTOF.

E. Correlation between the strength of pS6 signaling (median expression) and the sensitivity to DHODHi (-logIC50) in PDXs (n =14, $p = 0.0007$, $R^2 = 0.63$). IC50 values were determined at 72 hours. pS6 median value (arcsinh transformed) was determined by CyTOF.

F. Cellular features ranked by importance in predicting sensitivity to BAY-2402234 as selected by XGBoost in Pro-BII and Pre-BI cells from cell lines (n=8) and PDXs (n=11). The top 2 features (> 0.1) are highlighted in the purple.

G. UMAP plot to show the expression of pS6 and frequency of pS6+ cells after DHODHi treatment in Nalm16 cells (pS6+, first row) and PDX SJ45503 (pS6-, second row). Nalm16 and PDX cells collected before (Day 0) and after BAY-2402234 treatment for 3 and 6 days were profiled by CyTOF. live cells were used to generate UMAP plots. The frequency of pS6+ live cells were further indicated in UMAP plots. The coloring axis in UMAP is pS6 (S235/236).

Data in bar graph (A) are shown as median ± SD. Data in curves (B, C, E) are mean ± SD. Linear regression correlation was evaluated in F. The best fit line was shown with 95% confidence bands (dashed curves). *$p < 0.05$, **$p < 0.01$, ***$p < 0.001$.

Figure 6. DHODH inhibition prolongs survival of pS6+ B-ALL xenograft models

A. Half a million B-ALL cells were injected by tail vein in NSG mice. Starting on day +3 following injection, xenografts were treated daily with 5 mg/kg BAY-2402234 for 24 dosing days (5 days on, 2 days off). The treatment stopped at the 34th day after IV injection. Bioluminescence imaging (BLI) was performed once a week for 5 weeks.

B. Bioluminescent images of NSG mice at Day 10, Day 17, and Day 24 post engraftment with PDX SJ18305/Luc+ cells. Crossed-out mice indicate experimental mice excluded from the analysis due to death unrelated to leukemia (see methods).

C. Bioluminescent images of NSG mice at Day 24, Day 31, and Day 34 post engraftment with Nalm16/Luc+ cells.

D. Leukemia progression in SJ18305 xenografts by bioluminescence in DHODHi (red curve) treated and vehicle (black curve) mice (n=5 per group).

E. Leukemia progression in Nalm16 xenografts by bioluminescence in DHODHi (red curve) treated (n=4) and vehicle (black curve) mice (n = 5).

F. Leukemia progression in SJ45503 xenografts by bioluminescence in DHODHi (red curve) treated and vehicle (black curve) mice (n=5 per group).

G. Leukemia engraftment in DHODHi or vehicle-treated SJ18305 xenografts.

H. Spleen weight in SJ18305 PDX xenografts in DHODHi treated and vehicle group.

I. Survival of SJ18305 xenografts treated with DHODHi (red curve) and vehicle (black curve). Gray area indicates the dosing period.

J. Survival of Nalm16 xenografts treated by DHODHi (red curve) and vehicle mice (black curve). The gray area indicates the dosing period.

K. Model of pyrimidine dependency and sensitivity to DHODH inhibition in B-ALL. B-ALL cells characterized by active pS6 signaling (left) are glucose dependent for de novo pyrimidine synthesis and uridine production. Active signaling downstream of mTOR pathway activates S6-kinase which phosphorylates CAD, driving pyrimidine synthesis. Consequently, these cells are reliant on de novo pyrimidine synthesis, making them susceptible to inhibition by targeting DHODH. In contrast, cells lacking pS6 signaling (pS6-) do not depend on de novo pyrimidine synthesis and, therefore, show minimal response to DHODHi treatment. Data in primary samples suggests patients may contain a mixture of pS6+ and pS6- cells but that pS6+, DHODH active cells are associated with chemoresistance. The figure was created in Biorender. Data in panels D and E are mean ± SD tested for significance using a 2-way ANOVA mixed model followed by Sidak's test for multiple comparisons. Data in box plots (F,G) are mean ± SD; Welch's *t* test was used. The log-rank test was used for Kaplan-Meier curves (H). $*P < .05$, $**P < .01$, $***P < .001$, $****P < .0001$.

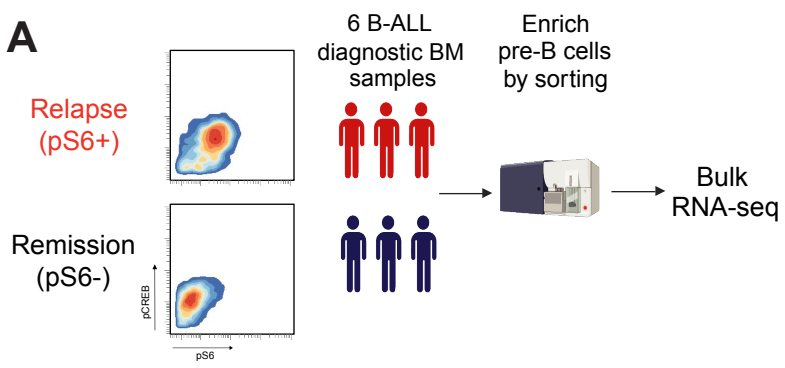

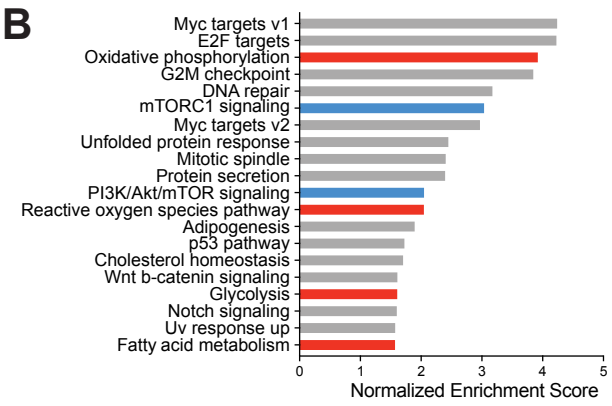

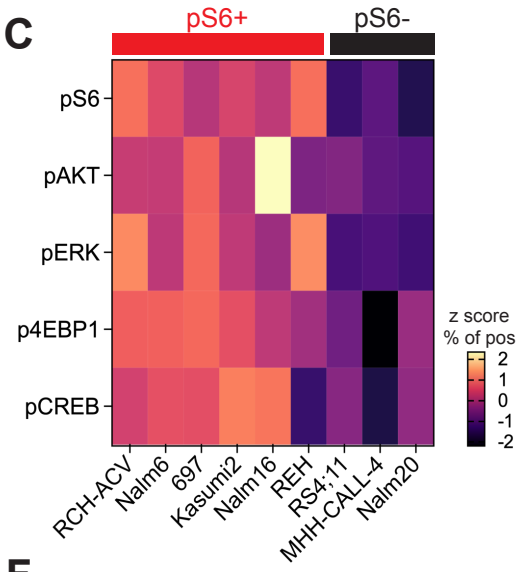

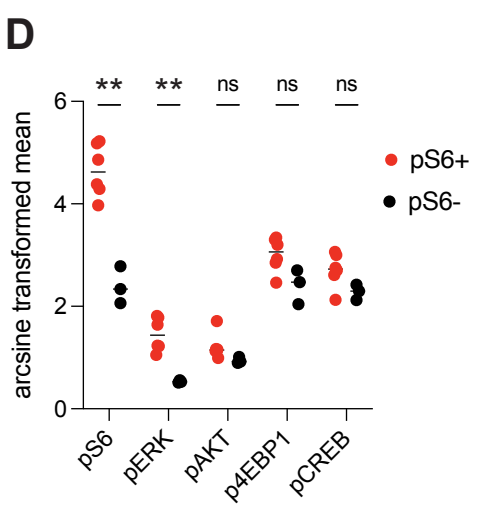

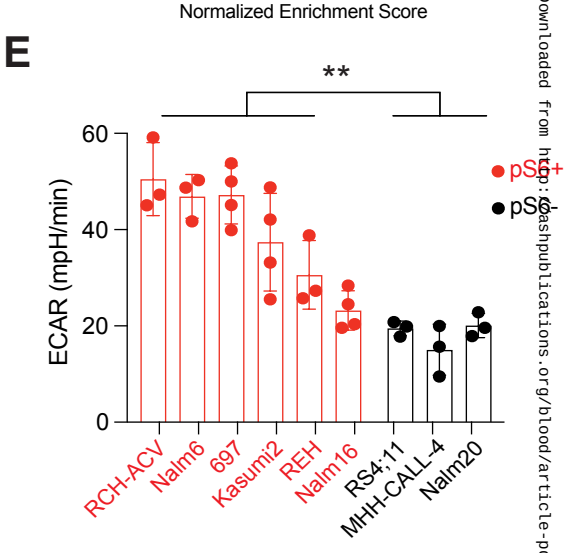

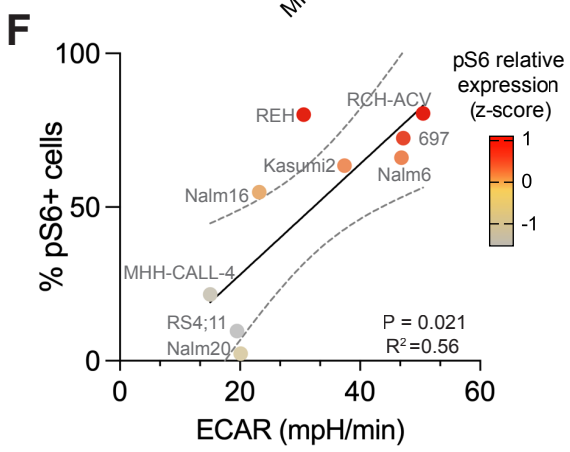

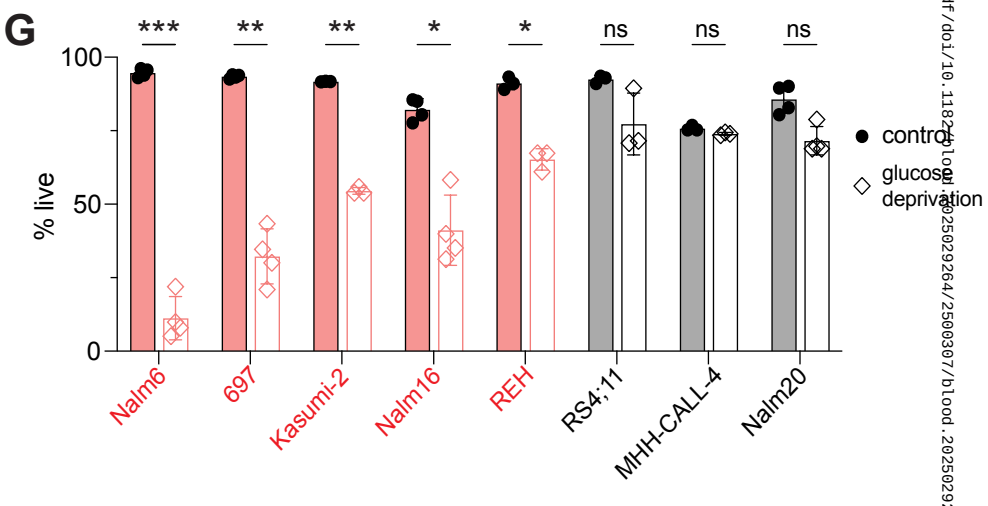

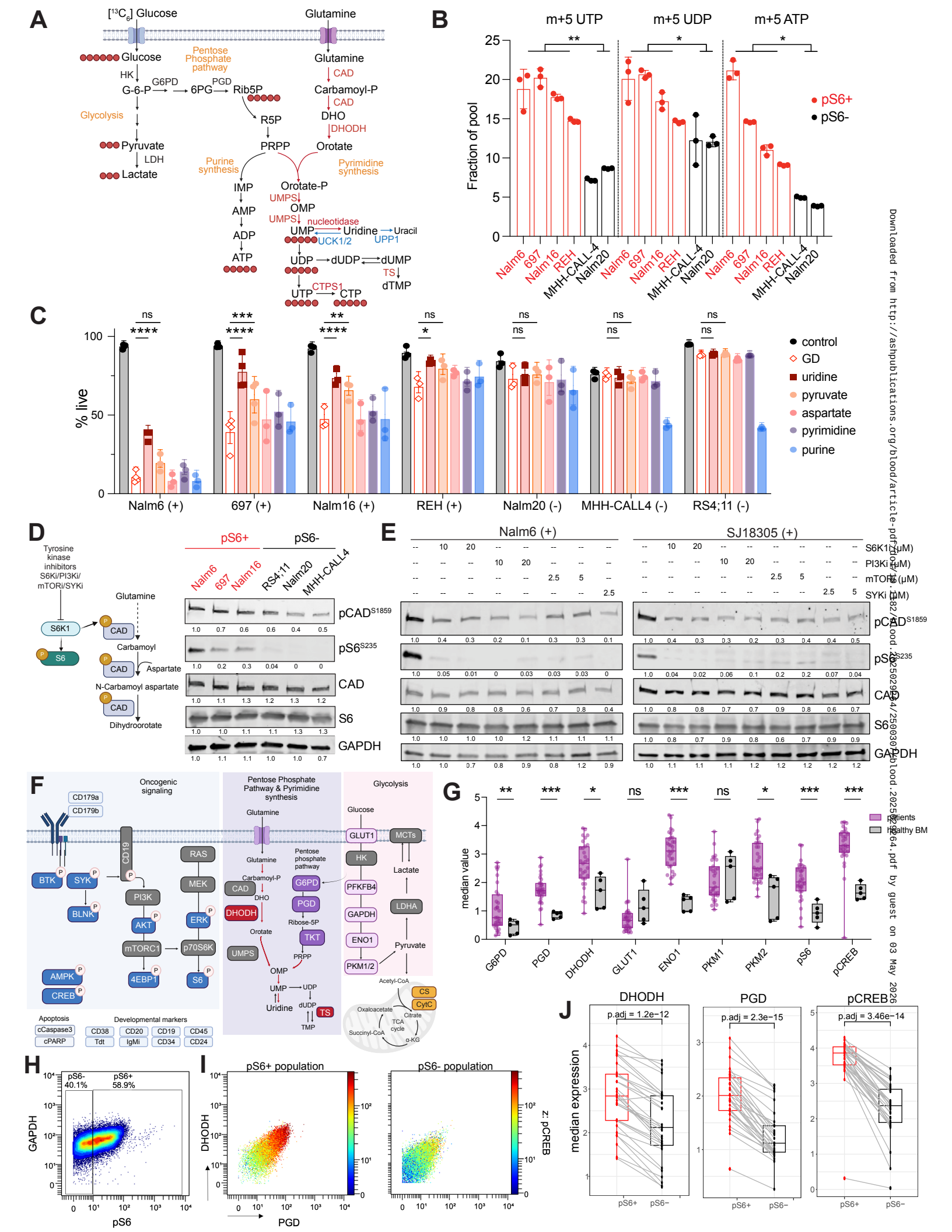

Figure 3

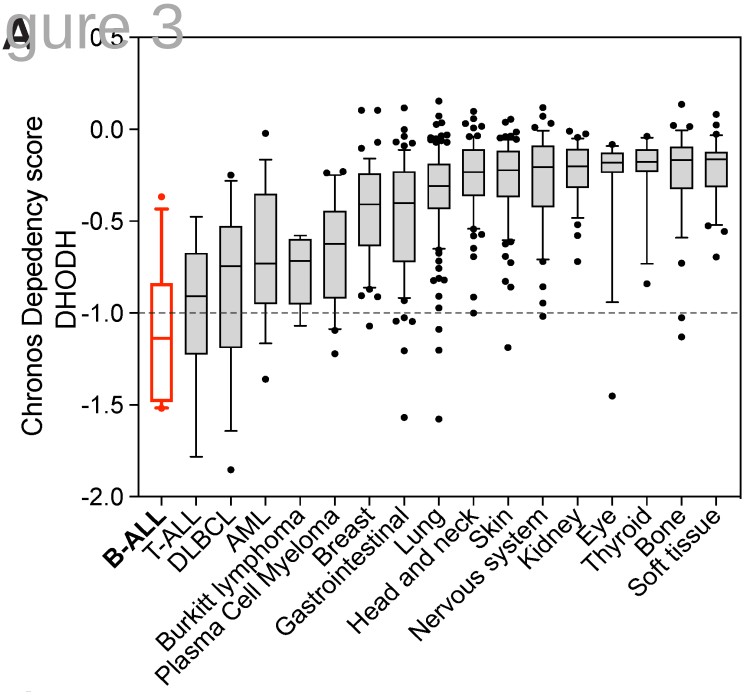

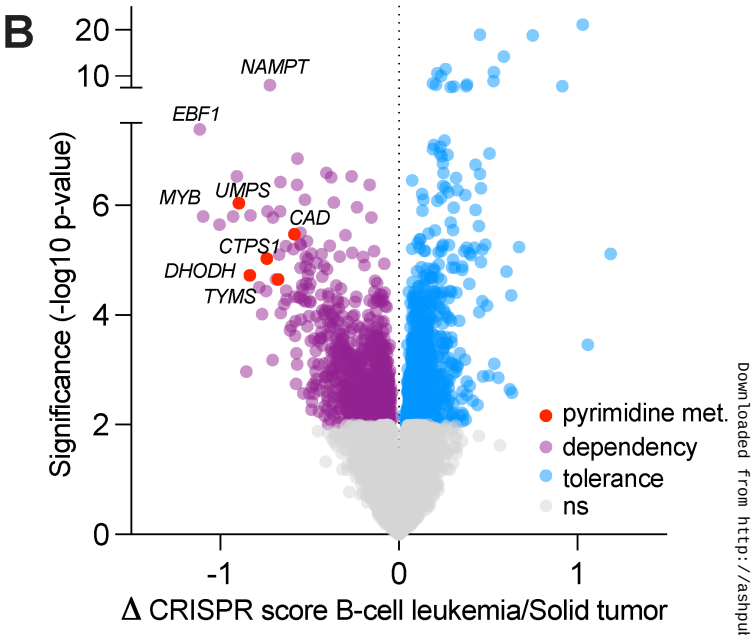

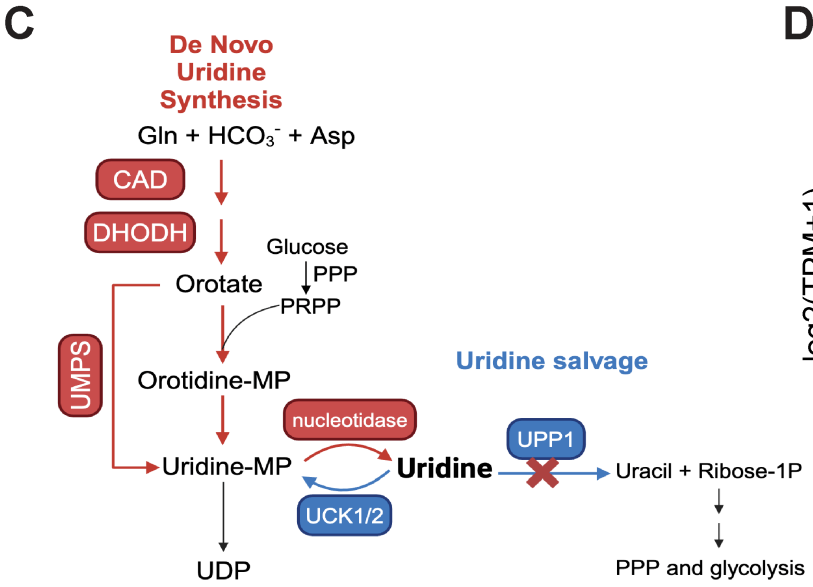

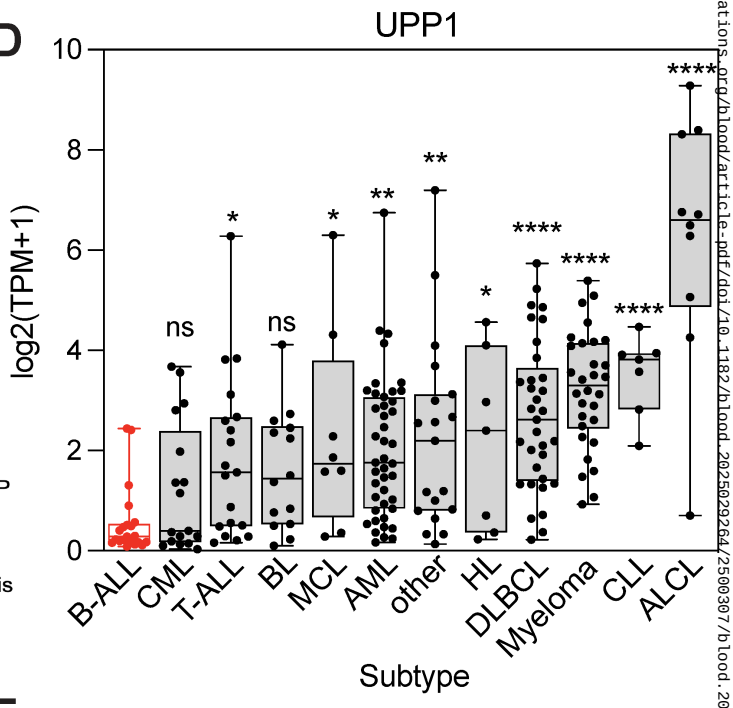

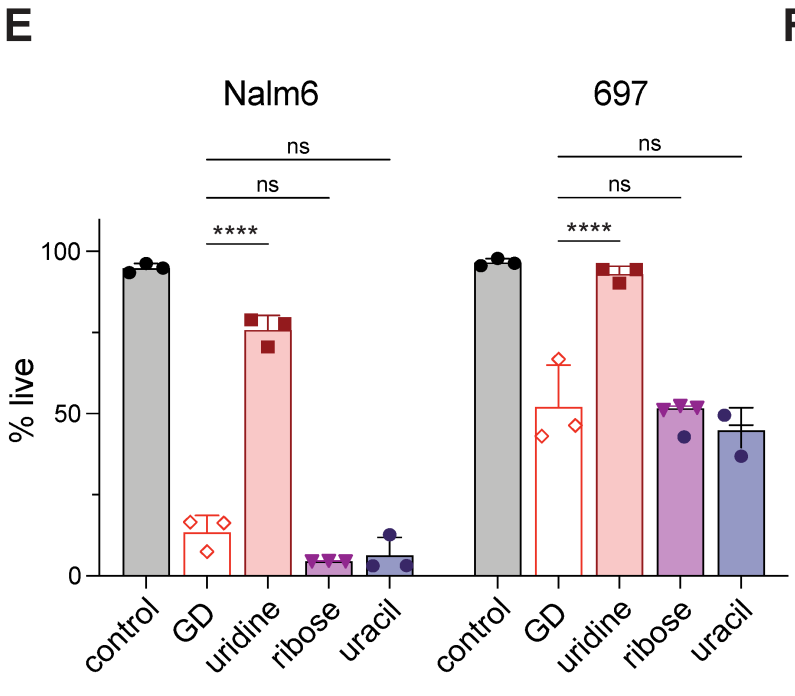

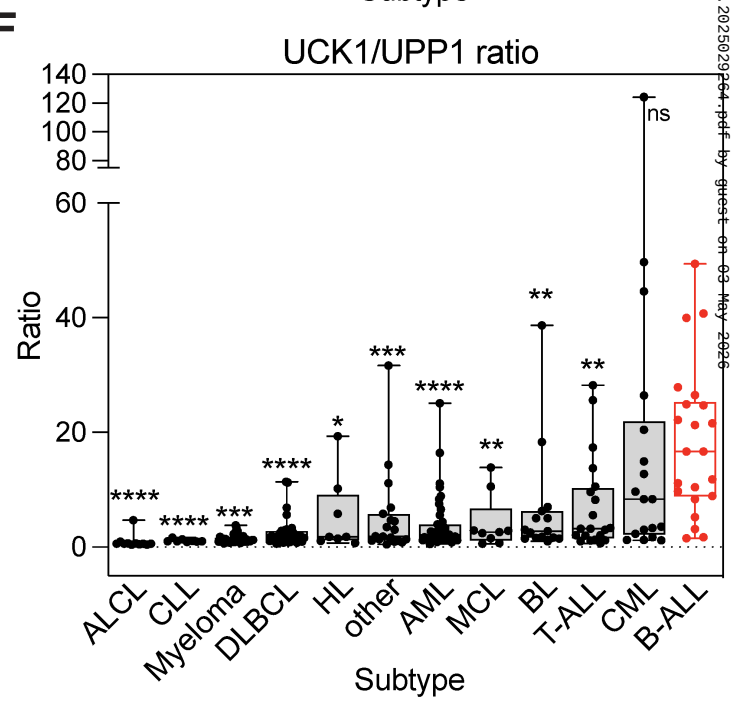

Figure 4

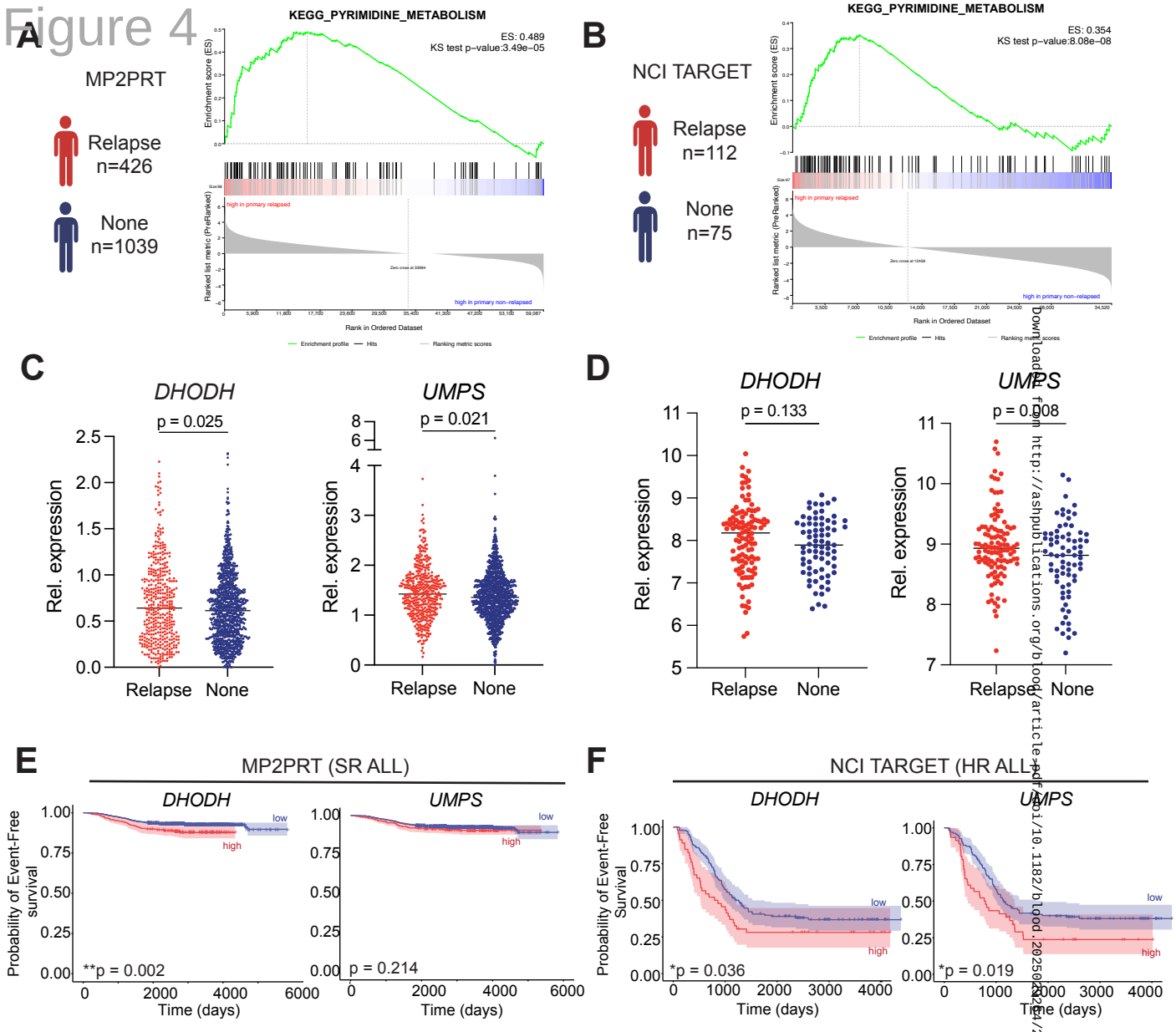

Figure 5

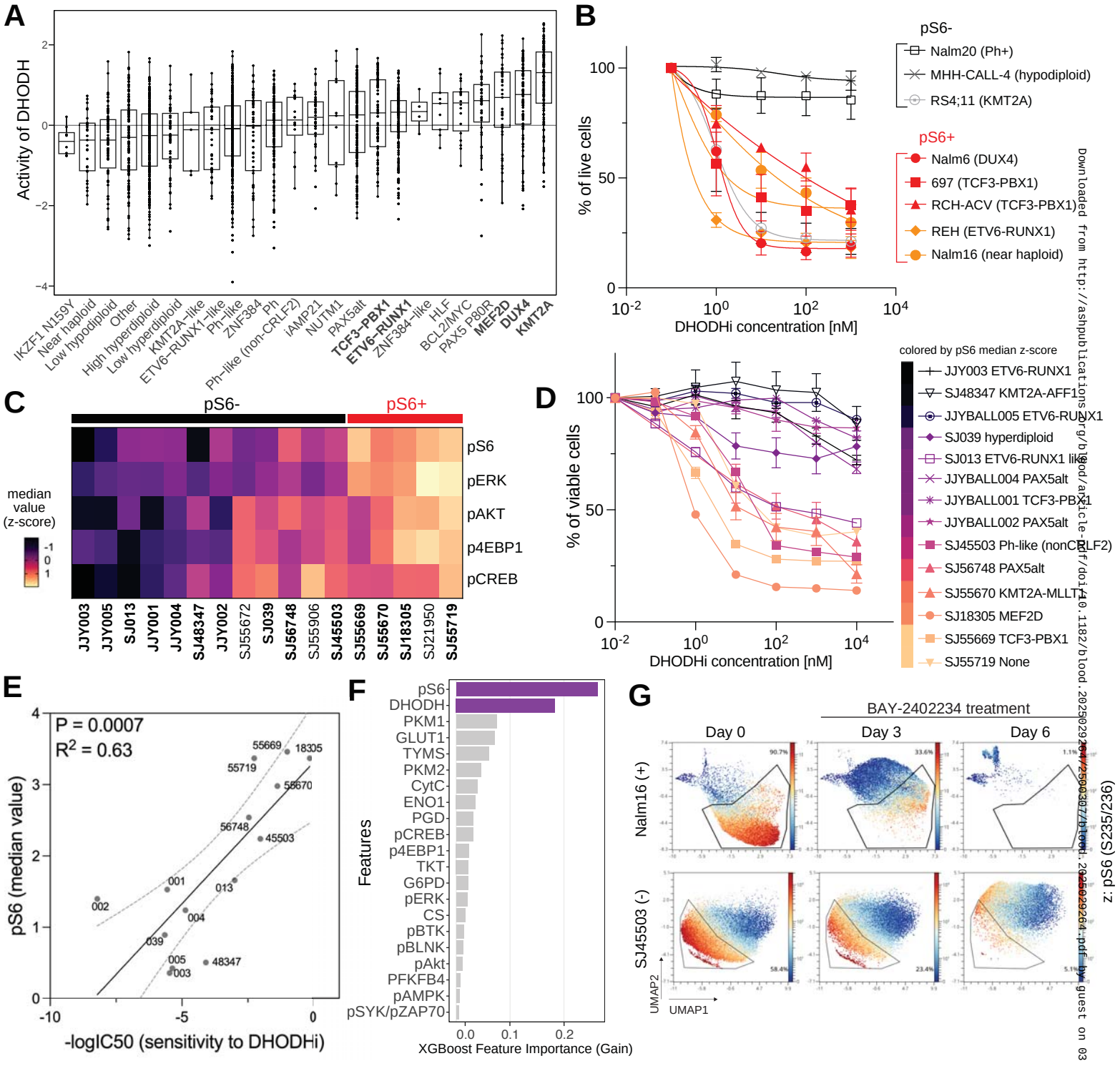

Figure 6

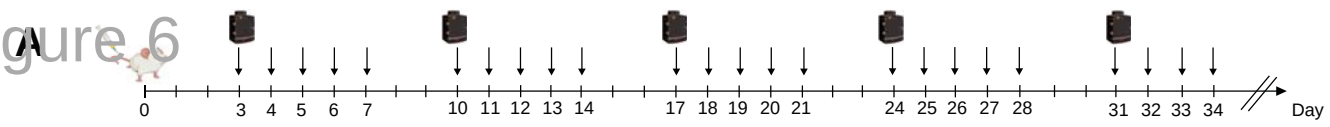

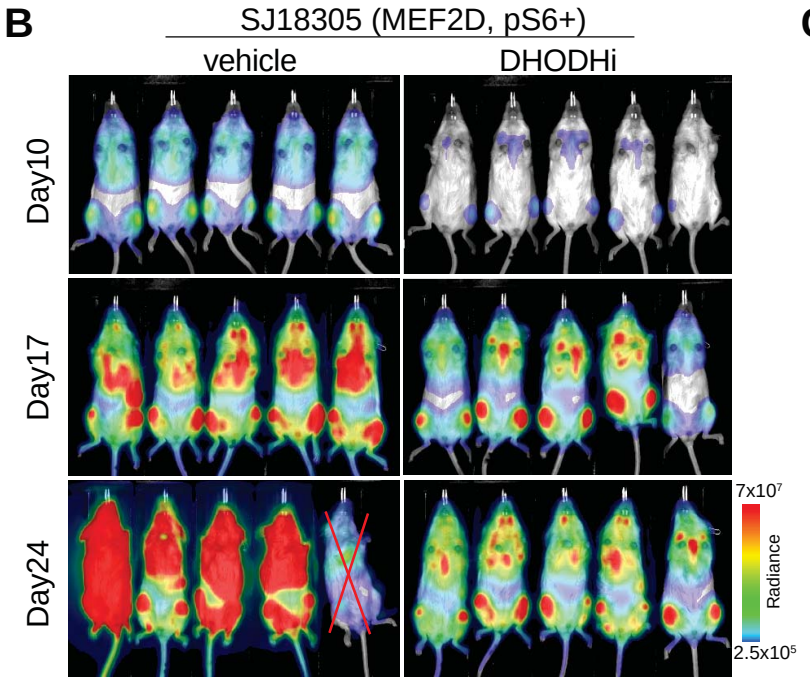

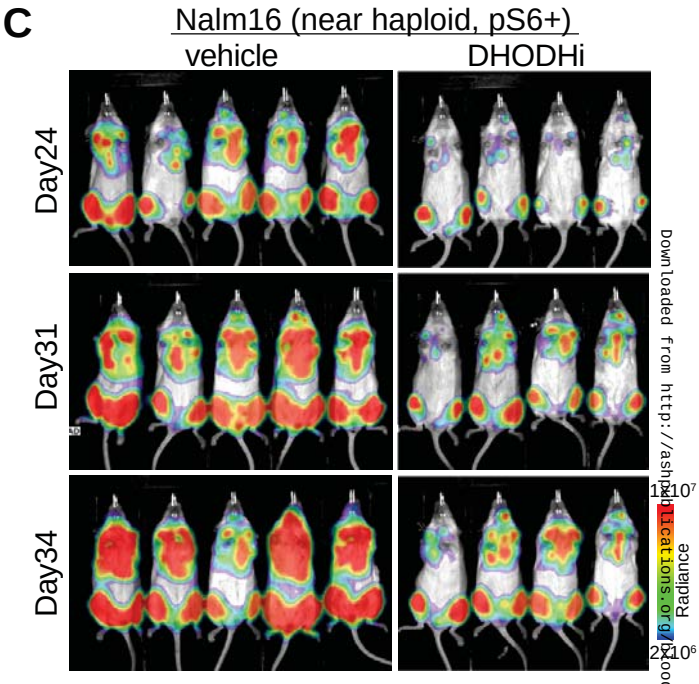

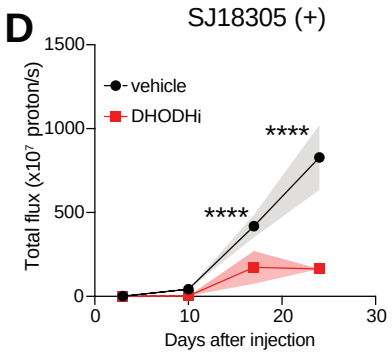

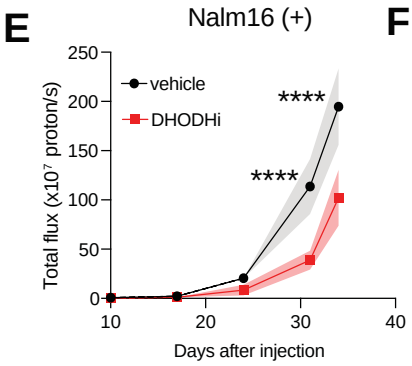

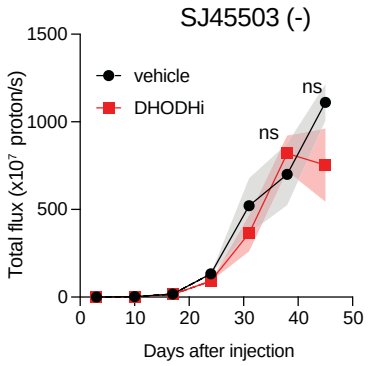

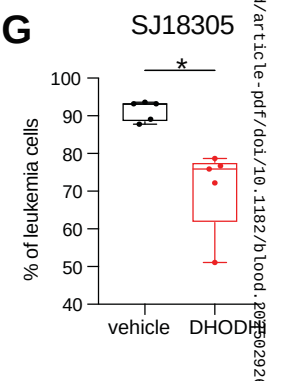

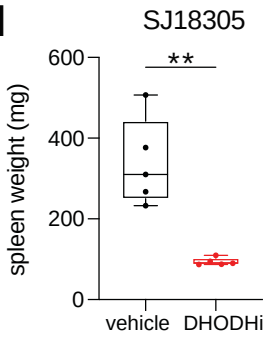

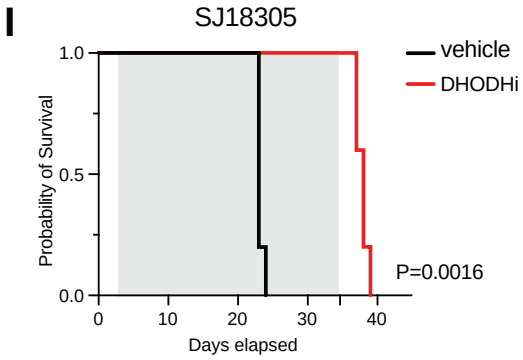

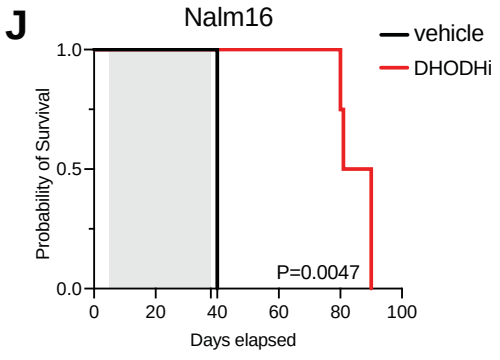

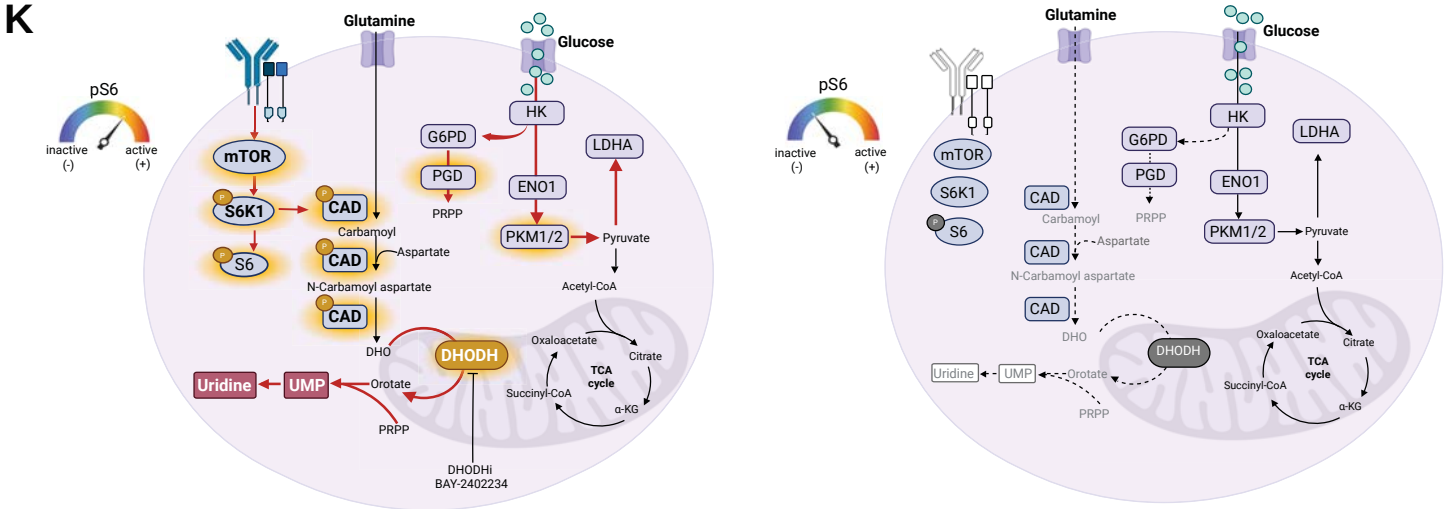

Dihydroorotate Dehydrogenase (DHODH) as a Targetable Metabolic Achilles' Heel for Chemo-Resistant B-cell Acute Lymphoblastic Leukemia (B-ALL)

Context of Research

Relapse in B-ALL is linked to active signaling pathways and high glucose use, but therapeutic targets distinguishing relapse from remission remain largely unexplored

Aim of This Study

To characterize relapse-associated mTOR-signaling active cells and study their metabolic dependency in patients with chemo-resistant B-ALL

Findings

Relapse-associated B-ALL cells with active mTOR signaling rely on de novo pyrimidine synthesis through regulating CAD, making them vulnerable to DHODH inhibition

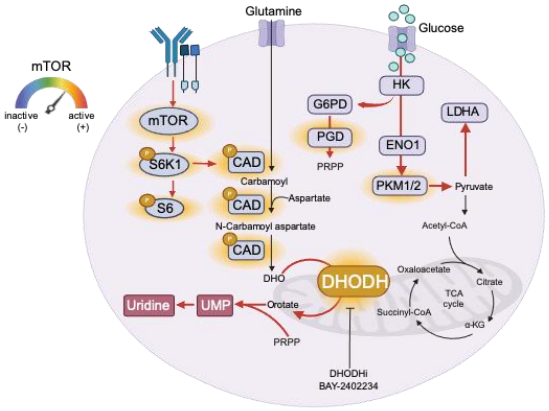

Across cancer, B-ALL is most dependent on de novo pyrimidine synthesis

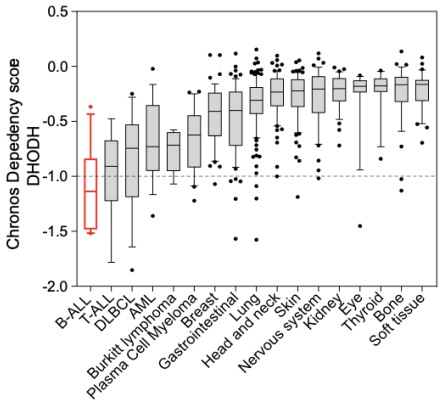

DHODH inhibition reduces leukemia burden and prolongs survival in CDX and PDX models *in vivo*

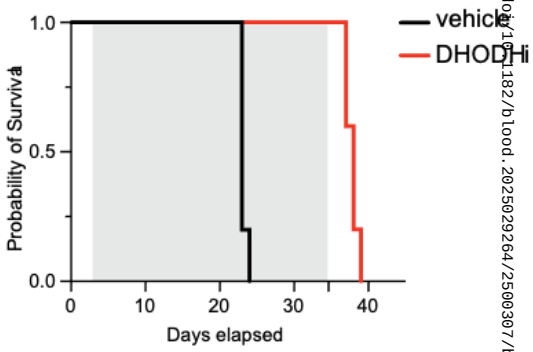

Figure was created in Biorender.

Conclusions: B-ALL cells with active mTOR signaling exhibit increased reliance on *de novo* pyrimidine synthesis. DHODH inhibition disrupts this metabolic dependency and demonstrates potent *in vitro* and *in vivo* efficacy, defining a targetable metabolic vulnerability and a potential therapeutic strategy for B-ALL.

*Liu et al. DOI: 10.xxxx/**blood**.2025xxxxxx*

blood Visual Abstract